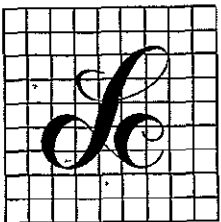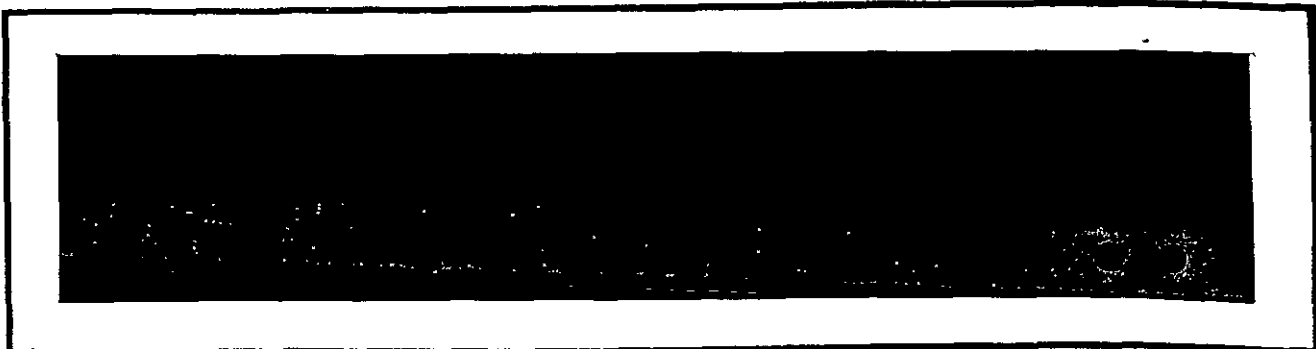NASA CR-

160537

LinCom Corporation

PO Box 2793D, Pasadena, Calif 91105

FINAL REPORT

PHASE III

SPS PILOT SIGNAL DESIGN AND POWER

TRANSPONDER ANALYSIS

VOLUME II

PREPARED FOR

NASA JOHNSON SPACE CENTER
HOUSTON, TX   77058

TECHNICAL MONITOR: JACK SEYL

PREPARED UNDER CONTRACT NO. NAS 9-15782

PREPARED BY

W. C. LINDSEY
R. A. SCHOLTZ
C. M. CHIE

LINCOM CORPORATION
P.O. BOX 2793D
PASADENA, CA 91105

JANUARY, 1980

TR-0180-0779

ACKNOWLEDGEMENT

LinCom

LinCom

LinCom

TABLE OF CONTENTS

LinCom

LinCom

TABLE OF CONTENTS Cont'd

PAGE

LinCom

SUMMARY

In this report, we address the problem of pilot signal parameter optimization and the related problem of power transponder performance analysis for the SPS reference phase control system. Signal and interference models are established to enable specifications of the RF front end filters including both the notch filter and the antenna frequency response. A simulation program package is developed to be included in SOLARSIM to perform tradeoffs of system parameters based on minimizing the phase error for the pilot phase extraction.

An analytical model that characterizes the overall power transponder operation is developed. From this model, the effects of different phase noise disturbance sources that contribute to phase variations at the output of the power transponders can be studied and quantified.

The important findings on the transponder design parameters and results can be summarized as follows:

    ○EIRP = 93.3 dBW

    ○PN Chip Rate $\sim$ 10 Mcps

    ○RF filter 3 dB cutoff frequency $\sim$ 20 MHz

    ○Notch filter 3 dB cutoff frequency $\sim$ 1 MHz

    ○Notch filter dc attenuation $\sim$ 60 dB

    ○PN Code period $\gtrsim$ 1 msec

    ○Costas loop phase jitter $\leq$ 0.1 deg for 10 Hz loop bandwidth

    ○PN Code loop jitter is negligible

    ○Channel Doppler is negligible

    ○Klystron phase control loop bandwidth $\geq$ 10 KHz

In conclusion our results indicate that it is feasible to hold the antenna array phase error to less than one degree per power module for the type of disturbances modeled in this report. However, there are irreducible error sources that are not considered herein and their effects remain to be seen. They include:

- Reference phase distribution errors
- Differential delays in the RF path

1.0 INTRODUCTION

This report serves to document results from the Pilot Signal Parameter Optimization/Analysis (Task I) and the Power Transponder Analysis/Modeling (Task II) of the SPS Antenna Phase Control System Hardware Simulation Study (Phase III). It can be divided into two parts: Sections 2.0 - 11.0 deal with Task I and Sections 12.0 - 15.0 are devoted to Task II.

The key technical issues to be addressed under Task I can be summarized by Fig. 1.1. The interferences are generated by the following mechanisms: (1) self jamming due to the power beam leakage from the diplexer/circulator; (2) mutual coupling from adjacent transponders and (3) thermal noise. The signal and interference spectrum at the input to the SPS transponder is depicted in Fig. 1.1(b). In general, the combined phase noise inference from the power beams consists of a coherent and a noncoherent term. Depending on the mechanization of the antenna structure and diplexer/circulator characteristics, these terms are associated with gains K_1 and K_2. Note that the phase noise interferences are concentrated around the carrier frequency (2450 MHz). The uplink pilot signal on the other hand has no power around this frequency. Its power spectrum peaks at $f \approx 0.75\ R_c$, with a value proportional to the product of the received power (P_R) and the PN chip rate (R_c), and inversely proportional to the PN code length (M). The parameters R_c and M are also related to the processing gain of the PN spread signal and determine its interference suppression capability. Notice also that about 14% of the pilot signal power lies between $|f| < 2R_c$. The RF filter characteristic is mainly determined by the waveguide antennas, which have bandwidths ranging
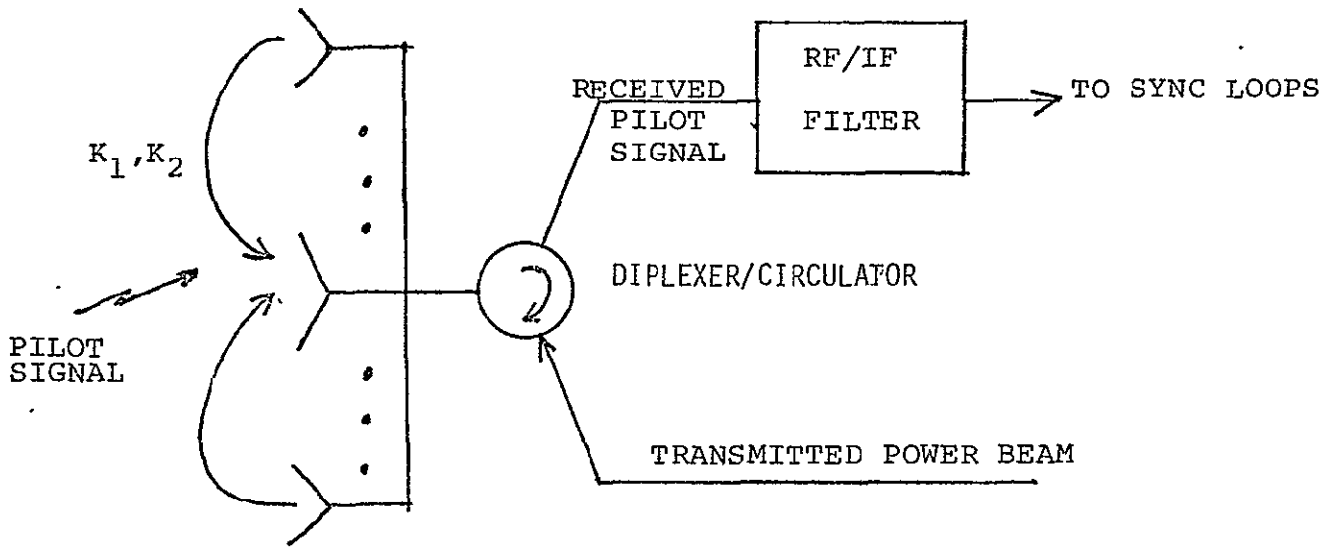
(a) SPS Power Transponder Front End
     (Conceptual)
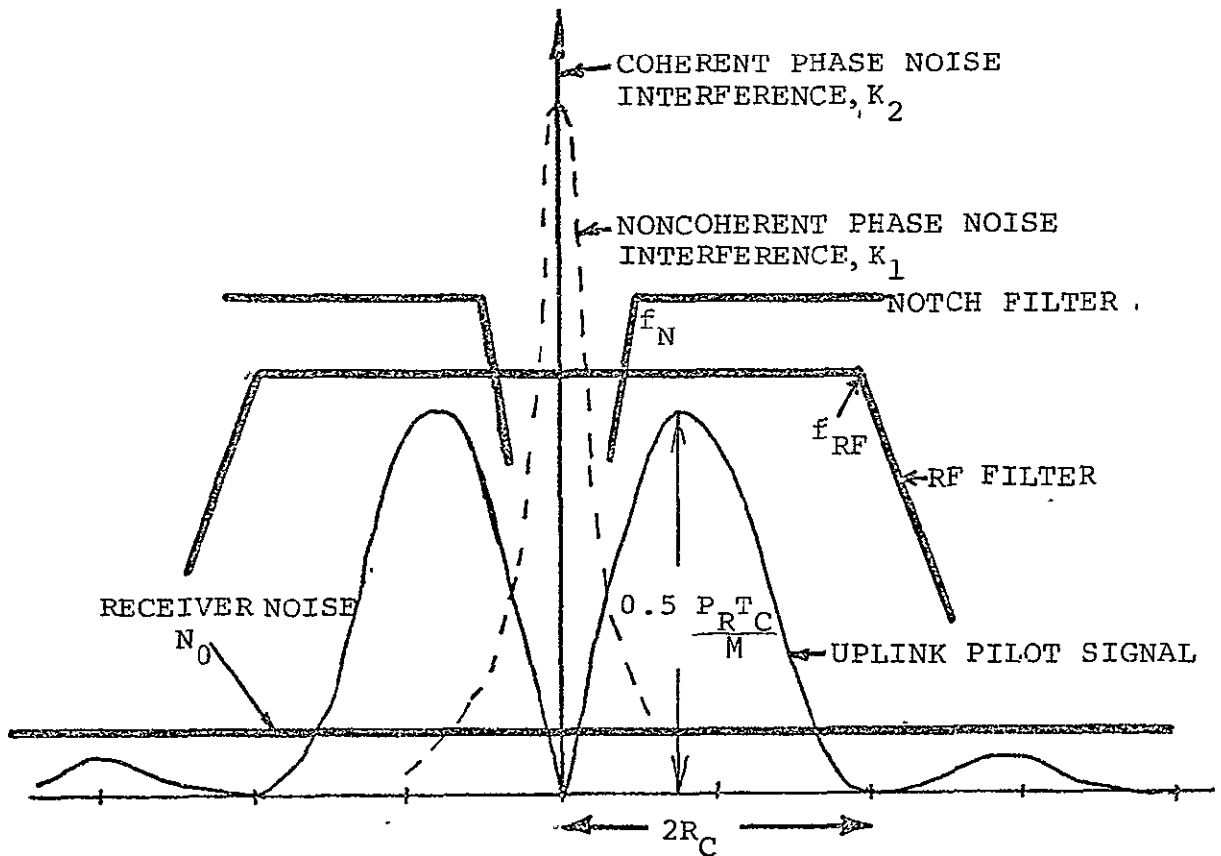
(b) Signal and Noise Spectrum

79 0254

Figure 1.1. Signal and Noise Spectrum into SPS Transponder.

from approximately 15 to 45 MHz depending on the array area. Our goal is to optimally select (1) the pilot signal so that it passes through the RF filter with negligible distortions, and (2) a practical notch filter that rejects most of the phase noise interferences. When this is done, one can be assured that the reconstructed pilot signal phase after the sync loops bears a tolerable error for the retrodirective scheme.

In this report, we have characterized the interference model and requirements for the optimization of the first IF filter for the pilot signal communication system. We have characterized analytically the power spectral density of the pilot signal as well as various sources of interference. From this information, we are able to optimize the first IF filter in the reference SPS transponder for interference rejection. We have also formulated a mathematical framework which serves as a basis where different tradeoffs can be made·in terms of system parameters such as pilot signal transmitter EIRP, PN code requirements and chip rates. Based upon this mathematical model, a computer program is developed to be included in the SOLARSIM package to perform tradeoffs of pertinent design parameters of the receiver portion of the SPS transponder; the phase error of the pilot phase tracking (Costas) loop is used as the performance measure. As a result of the SOLARSIM data, the following can be specified on a preliminary basis: (1) chip rate, (2) notch filter response, (3) code period, (4) uplink EIRP and (5) Costas loop bandwidth.

Under Task II, we have developed analytical models for the SPS transponder tracking loop system that includes: (1) the PN despreader loop, (2) the pilot phase tracking (Costas) loop and (3) the PA phase

control loop. The phase reference receiver that feeds the reference phase
distribution system is also modeled. Various sources of potential
phase noise interferences are identified and their effects on the
performance of the individual loops are modeled. In particular, a
model of the phase noise profile of the klystron amplifier based
on a specific tube measurement is introduced. Important implications
on the PA control loop design are also addressed.

An analytical model for evaluating the overall performance of the
SPS transponder is given. The phase fluctuation at the output of the
transponder is shown to be directly related to the various noise
processes through the closed-loop transfer functions of the tracking
loops. These noise processes are either generated externally to the
transponder circuitry such as ionospheric distrubances, transmit
frequency instability, or externally such as receiver thermal noise,
power beam interferences, data distortions, VCO/mixer phase noise
and the phase variations introduced by the reference distribution tree.
A detailed computer simulation is deemed necessary to quantitatively
investigate the interplays between the .elements of the transponder.
Based on our preliminary investigations, some recommendations on the
transponder design are also made.

2.0 THE PROBLEMS AND ASSUMPTIONS ASSOCIATED WITH SPS PILOT SIGNAL DESIGN OPTIMIZATION

We wish to design the pilot signal communication system to operate reliably in the face of several types of interference:

(1) The downlink power beam signal.

(2) Noise in the spacetenna receivers.

(3) Unintentional or intelligent RFI.

(4) Intelligent beam stealing signals.

Figure 2.1 illustrates the R.F. signal scenario under consideration. The spacetenna is composed of 101,552 variable size rectangular arrays which range from 1.73mx1.73m to 5.2mx5.2m, operating at a frequency of 2450 MHz.

The power beam signal contributed by the ith subarray is denoted by $s_i(t)$ for $i=1,2,\ldots,N$, measured at the output port of the ith transmitter. The signal at the output of the jth subarray's RF receiver is given by $r_j(t)$ and possesses components due to the power beam signals $s_i'(t)$, $i=1,\ldots,N$, the receiver noise $n_j(t)$, the RFI $s_{RFI}(t)$, and a possible beam-stealing signal $s_{BS}(t)$, in addition to the desired pilot signal $s_p(t)$. If we knew all of these input signals to the scenario, we could develop a representation for $r_j(t)$ as indicated in Figure 2.2, once we have the following additional information:

(a) The system function $H_{ij}(f)$ describing the coupling of the ith power beam signal to the jth receiver's RF output signal $r_j(t)$. This includes the effects of all waveguides, circulators, RF receiver filters, antennas, etc. This must be known for all values of i.

(b) The system function $H_{RF}(f)$ from the jth subarray's antenna terminal to the jth receiver's RF output signal $r_j(t)$. This

MASTER-SLAVE RETURNABLE TIMING SYSTEM

SIGNAL PROCESSOR #1

SIGNAL PROCESSOR #2

• • •

SIGNAL PROCESSOR #N

$r_1(t)$

$r_2(t)$

$r_N(t)$

X M I T #1

R C V R #1

$n_1(t)$

X M I T #2

R C V R #2

$n_2(t)$

X M I T #N

R C V R #N

$n_N(t)$

$s_1(t)$

$s_2(t)$

$s_N(t)$

SUBARRAY #1

SUBARRAY #2

SUBARRAY #N

S P A C E T E N N A

I O N O S P H E R E

A T M O S P H E R E

$s_{RFI}(t)$

RFI SOURCE

$s_P(t)$

PILOT SIGNAL XMTR

$r_{BS}(t)$

$s_{BS}(t)$

INTELLIGENT BEAM STEALER
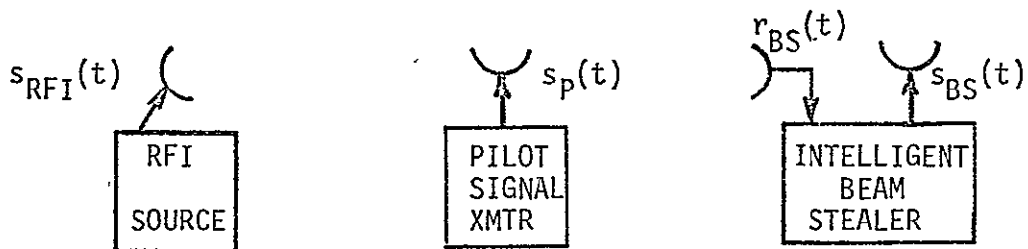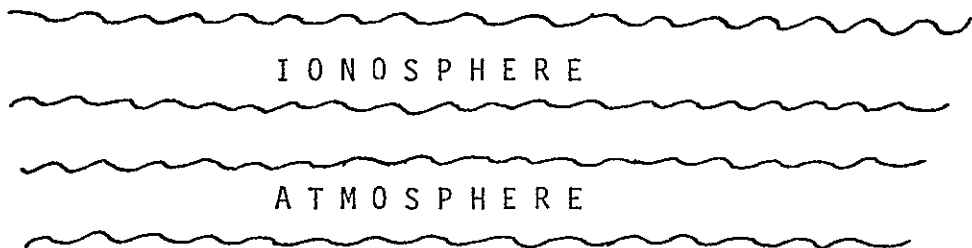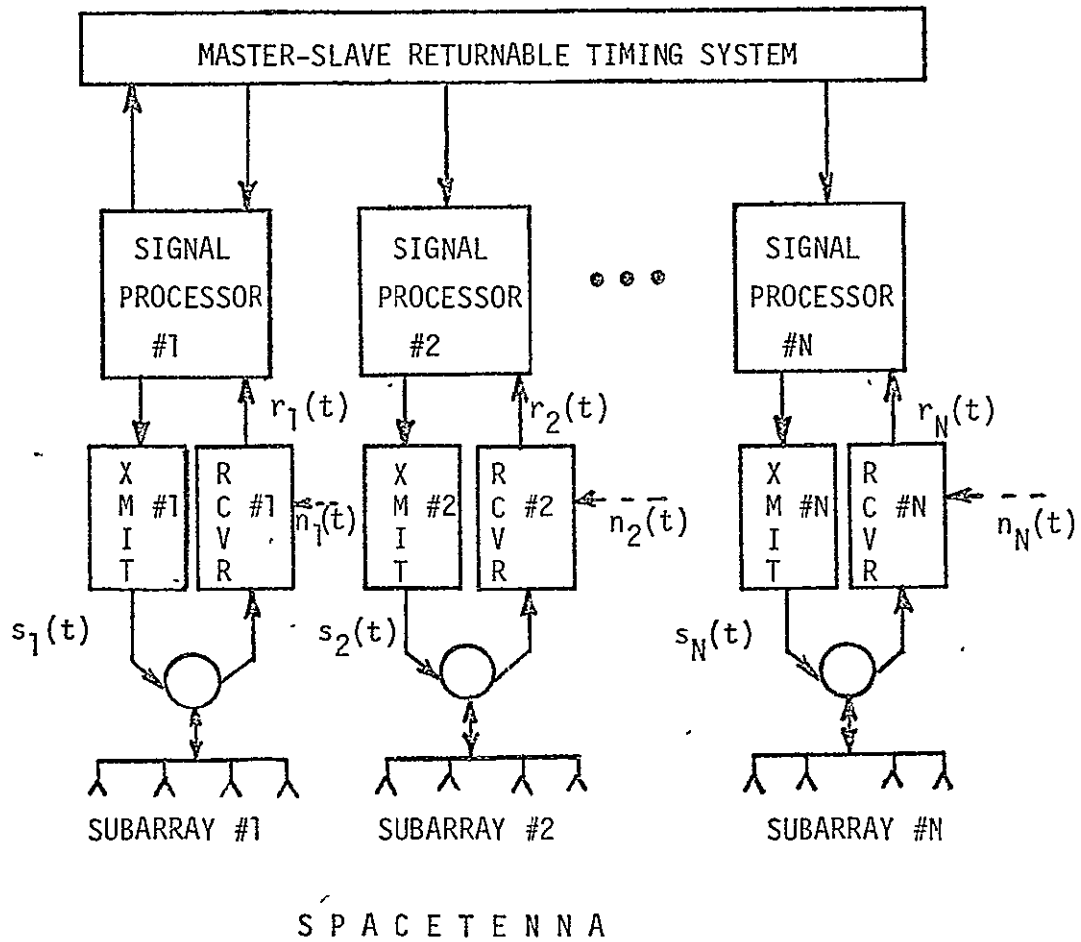
Figure 2.1. RF Signal Scenario.

79 0255

RECEIVER NOISE

COUPLING
FUNCTIONS

$n_j(t)$

$s_1(t) \longrightarrow H_{1j}(f)$

$s_2(t) \longrightarrow H_{2j}(f)$

$s_N(t) \longrightarrow H_{Nj}(f)$

$+$ (SUM AT MIXER INPUT)

$r_j(t) \longrightarrow$ TO $j^{\underline{th}}$ SIGNAL PROCESSOR

$H_{RF}(f)$ SUBARRAY RECEIVER RF SYSTEM FUNCTION

ATMOSPHERIC & IONOSPHERIC CHANNELS

$s_{RFI}(t) \longrightarrow$ RFI CHANNEL

$s_P(t) \longrightarrow$ PILOT SIGNAL CHANNEL

BEAM STEALING PROCESSOR

$s_{BS}(t) \longrightarrow$ BEAM STEALING CHANNEL

$+$ (SUM AT ANTENNA TERMINAL)

Figure 2.2. Received Signal Generation.

also includes the effects of waveguides, circulator, RF

filters, etc.

(c)   Atmospheric and ionospheric channel models for the paths

from the pilot signal transmitter, the RFI source, and

the beam stealer to the antenna terminal of the $j\underline{th}$ subarray.

(d)   A "threat model" indicating the capabilities and level of

sophistication of the beam stealing processor.

Knowledge of the above quantities would make the analyses to

follow more precise.

The pilot signal baseline design [1] is given as NRZ/BPSK/

Bi-ϕ-DS/CDMA, i.e.,

$$s_p(t) = \text{Re}\{d(u,t)c(u,t)a(u,t)e^{j\omega_c t}\}$$

where u is a sample space parameter indicating randomness, $d(u,t)$ is

an NRZ binary data signal BPSK modulated on a Manchester-coded

direct-sequence spread spectrum signal, and $a(u,t)$ represents
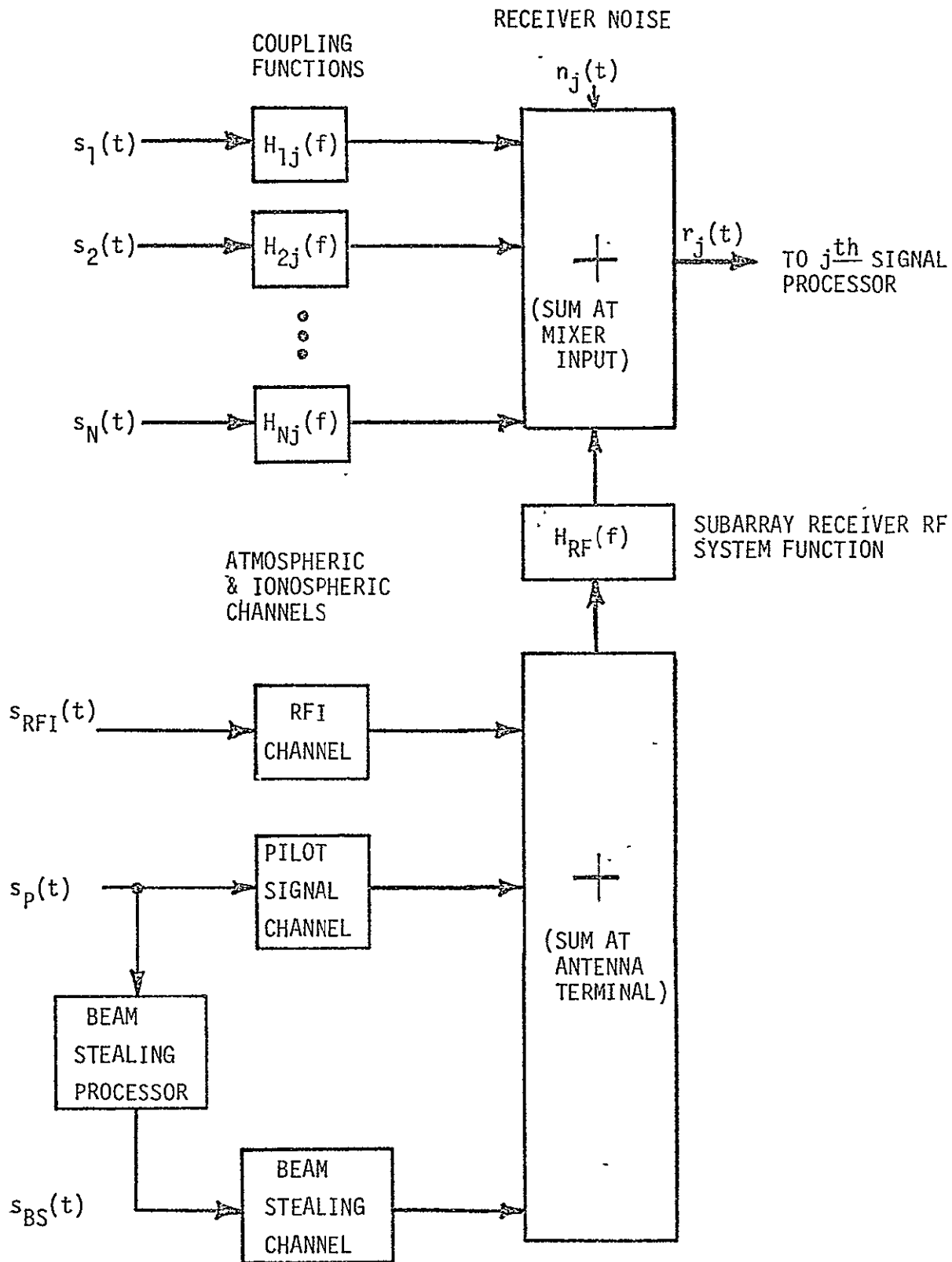
(unwanted) amplitude and phase modulation on the pilot transmitter.

We assume that the following approximations are valid:

(a)   The atmospheric-ionospheric channel can be modelled as:

(SIGNAL AT PILOT $b(u,t)$ (SIGNAL AT SUBARRAY
TRANS. OUTPUT)   APERTURE)
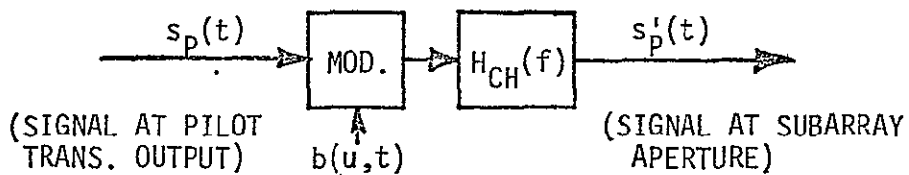
$$s_p'(t) = \int_{-\infty}^{\infty} h_{CH}(t-t')\text{Re}\{d(u,t')c(u,t')a(u,t')b(u,t')e^{j\omega_c t'}\}dt'$$

(b)   The filtering $H_{CH}(f)$ imposed by the channel is wide

compared to the receiver RF filtering $H_{RF}(f)$. Assuming

that attenuation functions which are uniform across the

bandwidth of $H_{RF}(f)$ are included in the channel fading
function $b(u,t)$, we approximate $h_{CH}(t)$

$$h_{CH}(t) = \delta(t-\tau(u))$$

by a pure random delay. Therefore

$$s_p'(t) = Re\{m'_p(t-\tau(u))e^{j\omega_c t}\}$$

$$m_p'(t) = a(u,t)b(u,t)c(u,t)d(u,t)$$

(c) The RF and IF sections of the subarray receivers are
modelled in Figure 2.3. Under weak narrowband assumptions
we can reduce the RF and IF subsystem signal processing
model to an equivalent complex baseband signal processing
model. These techniques are discussed in Appendices 1
and 2. The resultant model is shown in Figure 2.4. If $s(t)$
is the input signal in Figure 2.3, then $m_x(t)$ is the
equivalent input signal in Figure 2.4 where

$$x(t) = Re\{m_x(t)e^{j\omega_c t}\}$$

The output signal $y(t)$ and its baseband equivalent $m_y(t)$
are related by

$$y(t) = Re\{m_y(t)e^{j\omega_{IF} t}\}$$

where the IF frequency is 490 MHz which is one-fifth
of the carrier frequency.

(d) We further assume that the factor $a(u,t)b(u,t)d(u,t)$
of the received pilot signal's modulation is quite narrow
band relative to the passband of the equivalent RF system
function $G_{RF}(f)$. The product filtering approximation of
Appendix 3 can then be applied to further simplify the effect
of the RF filter on the received pilot signal.

OUTPUT
TO PN
SYNC SYSTEM

RF SYSTEM
FUNCTION

IF
MIXER

FIRST IF
FILTER

SECOND IF
FILTER

INPUT

$H_{RF}(f)$

$H_1(f)$

$H_2(f)$

OUTPUT

INCIDENT
ELECTRIC
FIELD IN
SUBARRAY
APERTURE

TO CARRIER SYNC
AND DATA DEMOD
SYSTEMS

$\cos(.8\omega_c t + \theta(u,t))$
FROM CARRIER SYNC
SYSTEM

$c_R(u, t-\hat{\tau}(u))$
FROM PN SYNC
SYSTEM
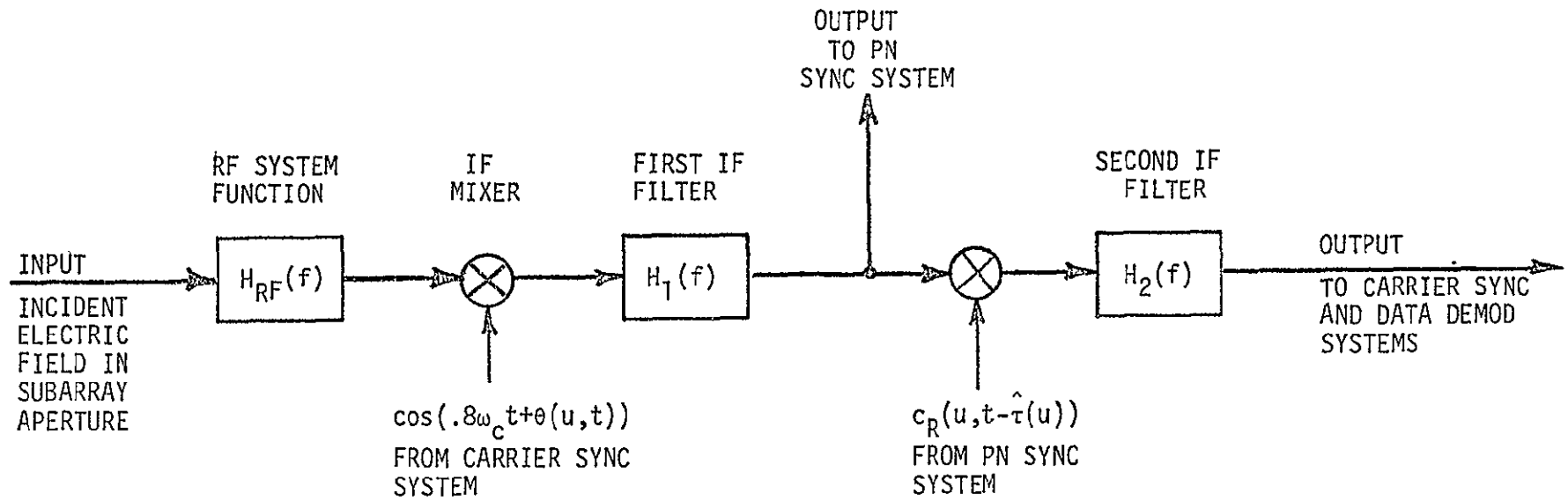
Figure 2.3. RF and IF Subsystem Signal Processing.

TO SYNC
CIRCUIT

EQUIVALENT
INPUT

SIGNAL AT
ANTENNA TERMINAL

$G_{RF}(f)$

$e^{j\theta(u,t)}$

$G_1(f)$

$c(u,t-\hat{\tau}(u))$

$G_2(f)$

EQUIVALENT
OUTPUT

TO CARRIER TRACK
AND DATA DEMOD SYSTEMS
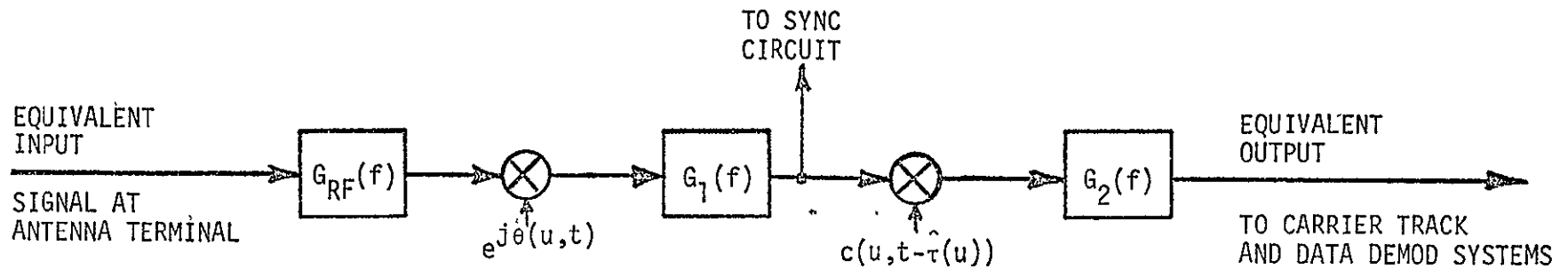
$$G_{RF}(f) = U(f+f_c)H_{RF}(f+f_c)$$

$$G_1(f) = U(f+f_{IF})H_1(f+f_{IF})$$

$$G_2(f) = U(f+f_{IF})H_2(f+f_{IF})$$

Figure 2.4. Complex Baseband Equivalent Circuit for the RF and IF Processor.

3.0 POWER SPECTRAL DENSITY COMPUTATIONS

We will now sketch the computation of the power spectral density at the input to the second IF filter. This is useful information for determining carrier tracking loop and ·data detector performance. The PN tracking loop contains a similar signal and these computations can be adapted to those design needs as well. We assume that superposition is valid and analyze each signal source's effect separately. We feel that this is a very good assumption despite the number of tracking loops which feed very slowly varying functions of the IF signal back into the system. These loops are "broken" in our computation.

3.1 The Pilot Signal

The Bi-φ DS spread spectrum (SS) modulation c(u,t) on the pilot signal is of the form

$$c(u,t) \; = \; \sum_{i} \; a_i P(t-iT_c-\delta(u))$$

where a_i is a known ±1 binary sequence, $\delta(u)$ is a random delay, T_c is the chip time, and P(t) is the basic Bi-φ waveform:
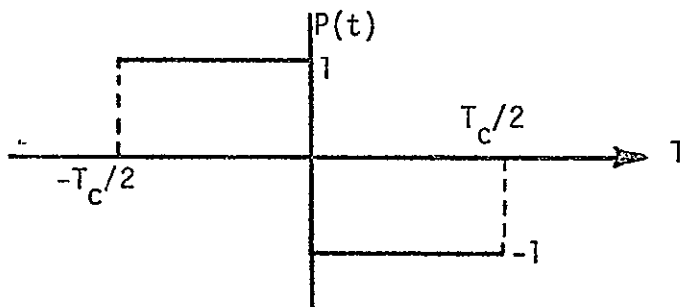
The chip time T_c and the sequence $\{a_i\}$ are design variables.

Pure power spectral analysis <u>cannot</u> be used to analyze the effect of the RF filter on the pilot signal. This is based on the fact that the <u>phase</u> of the SS code on the pilot signal relative to the <u>phase</u> of the code reference signal from the PN tracking loop

determines the bandwidth occupancy of this pilot signal component of the input to the second IF filter.

When $s_p^!(t)$ passes through the RF and first IF filters, we assume that the main effect of these operations is the reshaping of $P(t)$. Hence the output of the first IF filter is

$$s_p^{(1)}(t) \;\dot{=}\; \mathrm{Re}\{m_p^{(1)}(t-\tau(u))e^{j\omega_{IF}t}\}$$

where

$$m_p^{(1)}(t) \;=\; a(u,t)b(u,t)c^{(1)}(u,t)d(u,t)e^{j\theta(u,t+\tau(u))}$$

$$c^{(1)}(u,t) \;=\; \sum_i a_i Q(t-iT_c-\delta(u)) \quad.$$

and the new pulse shape $Q(t)$ is given by

$$Q(t) \;=\; P(t)*g_{RF}(t)*g_1(t) \quad.$$

Here $g_{RF}(t)$ and $g_1(t)$ are the impulse responses of the first two filters in the complex baseband equivalent circuit (Figure 4), and $*$ denotes convolution.

After PN code reference multiplication, the baseband equivalent input to the second IF filter is:

$$m_p^{(2)}(u,t) \;=\; m_p^{(1)}(t-\tau(u))c_R(u,t-\hat{\tau}(u))$$

$$=\; A(u,t)c^{(1)}(u,t-\tau(u))c_R(u,t-\hat{\tau}(u))$$

where $A(u,t)$ now represents the low bandwidth signal:

$$A(u,t) \;=\; a(u,t-\tau(u))b(u,t-\tau(u))d(u,t-\tau(u))e^{j\theta(u,t)}$$

(We in fact assumed earlier that $A(u,t)$ has bandwidth $\ll 1/T_c$.)

Now $c_R(u,t)$ is a replica of $c(u,t)$ except that the transmitter clock error $\delta(u)$ is not known.

$$c_R(u,t) = \sum_i a_i P(t-iT_c)$$

The product of SS signals appearing in $m_p^{(2)}(u,t)$ is then

$$c^{(2)}(u,t) \triangleq c^{(1)}(u,t-\tau(u))c_R(u,t-\hat{\tau}(u))$$

$$= \sum_i a_i Q(t-iT_c-\delta(u)-\tau(u))$$

$$x \sum_j a_j P(t-jT_c-\hat{\tau}(u))$$

$$= \sum_k c_k^{(2)}(u,t)$$

where

$$c_k^{(2)}(u,t) = \sum_j a_j a_{j+k} Q(t-(j+k)T_c-\delta(u)-\tau(u))P(t-jT_c-\hat{\tau}(u))$$

In the ideal processor from the pilot signal's point of view, the RF filter does not distort the pulse, i.e. $Q(t) = P(t)$, the PN sync subsystem adjusts $\hat{\tau}(u) = \tau(u)+\delta(u)$, and hence we would have

$$c^{(2)}(u,t) = c_0^{(2)}(u,t) = 1 \quad \text{(Ideal Pilot Signal Reception)}$$

Due to RF filter distortion and PN tracking error, $c_0^{(2)}(u,t)$ will be a periodic waveform with period T_c. One period of the waveform (between $-T_c/2 + \hat{\tau}(u)$ and $T_c/2 + \hat{\tau}(u)$) is given by $P(t-\hat{\tau}(u))Q(t-\delta(u)-\tau(u))$. Lets expand this waveform in a Fourier series to determine its harmonic content:

$$c_0^{(2)}(u,t) = \sum_n p_n(u)\exp(j2\pi nt/T_c)$$

where

$$p_n(u) = \frac{1}{T_c} \int_{-T_c/2+\hat{\tau}(u)}^{T_c/2+\hat{\tau}(u)} P(t-\hat{\tau}(u))Q(t-\delta(u)-\tau(u))\exp(-j2\pi nt/T_c)dt$$

$$= \frac{\exp\left(-\frac{j2\pi n\hat{\tau}(u)}{T_c}\right)}{T_c} \int_{-T_c/2}^{T_c/2} P(t)Q(t-e(u))\exp(-j2\pi nt/T_c)dt$$

and the PN <u>apparent</u> tracking offset is given by

$$e(u) = \tau(u) + \delta(u) - \hat{\tau}(u)$$

We call this the apparent tracking error for two reasons:

(1) Ideally we would like the PN tracking loop to drive
e(u) to the value which maximizes $|p_0(u)|$ to get the
maximum energy into the narrow 2nd IF filter and later
detection filters. This maximum may not occur at e(u)=0.

(2) The fact that P(t)≠Q(t) and Q(t) is not generally symmetric
in any way implies that the "S-curve" of the PN tracking
loop will not generally be symmetric or have a zero at
e=0.

As indicated in (1) above, we have identified a portion of the pilot
signal which corresponds to the desired 2$^{\underline{nd}}$ IF filter input, namely
the signal whose complex baseband representation is given by

$$m_p^{(3)}(u,t) \triangleq c_0^{(2)}(u,t)A(u,t)$$

$$\approx p_0(u)A(u,t)$$

The last approximation is quite accurate as far as 2$^{\underline{nd}}$ IF filter
computations go, since the other spectral components of $c_0^{(2)}(u,t)$
shift the spectrum of A(u,t) away from the filter passband by integer

multiples of $1/T_c$.

The remaining components $c_k^{(2)}(u,t)$, $k \neq 0$, of $c^{(2)}(u,t)$ correspond to signals modulated at the chip rate by the sequences $\{a_j a_{j+k}\}$; and hence are still spread spectrum signals. We view these as distortion noise and define their baseband equivalent signal as

$$n_p^{(3)}(u,t) \triangleq A(u,t) \sum_{k \neq 0} c_k^{(2)}(u,t)$$

The sum signal has period MT_c where M is the period of the sequence $\{a_j\}$ and can be analyzed spectrally once the design parameters are selected. For now we assume that the power in $n_p^{(3)}(u,t)$ which is in the passband of the IF filter is lower than that of $m_p^{(3)}(u,t)$ by at least the processing gain of the SS system. Hence is is not a major factor in the preliminary design and will be ignored.

At this point power spectral density calculations are quite easily done for the equivalent baseband pilot signal $m_p^{(3)}(t)$. Let us generally define

$$R_x(\tau) = <E\{x(u,t+\tau)x^*(u,t)\}>$$

and

$$S_x(f) = \int_{-\infty}^{\infty} R_x(\tau)\exp(-j2\pi f\tau)d\tau$$

We assume that the data modulation $d(u,t)$ is independent of $B(u,t)$ where

$$B(u,t) = a(u,t)b(u,t)e^{j\theta(u,t+\tau(u))}$$

But $\theta(u,t)$ cannot be considered independent of $a(u,t)$ and $b(u,t)$ whose phases it is designed to track. Continuing then,

$$m_p^{(3)}(u,t) = p_0(u)B(u,t)d(u,t)$$

and

$$S_{m_p^{(3)}}(f) = E\{|p_0(u)|^2\}S_B(f)*S_d(f)$$

3.2 Independent Interference

One of the major advantages of SS systems is their relative immunity to wide-sense stationary interference. There are several sources of interference which are independent of the SS code reference signal $c_R(u,t)$:

1.   Receiver noise $n_j(u,t)$.

2.   Unintentional RFI (we exclude multipath and intelligent jamming from this category).

3.   Downlink signals $s_j(t)$, $j=1,2,\ldots,N$.

The theory of wide-sense stationary independent interference rejection is covered in [2].

In general if a narrowband signal $s(u,t)$ is represented by a complex baseband equivalent signal $m_s(u,t)$, i.e.,

$$s(u,t) = Re\{m_s(u,t)e^{j\omega_c t}\}$$

Then the power spectral density of $m_s(u,t)$ can be determined from the corresponding density of $s(u,t)$ by

$$S_{m_s}(f) = 4U(f+f_0)S_s(f+f_0)$$

or, reversing the relation,

$$S_s(f) = \frac{1}{4}[S_{m_s}(f-f_0) + S_{m_s}(-f-f_0)]$$

We assume that we can determine the following power spectral densities:

1. $S_{n_j}(f) = N_0/2 =$ equivalent noise power spectral density. of the receiver reference to the antenna terminals.

2. $S_{RFI}(f) =$ the RFI power spectral density measured at the subarray antenna terminals. We assume that the effects of the RFI channel have been taken into account already.

3. $S_{s_j}(f) =$ the power spectral density of the output of the j-<u>th</u> subarray transmitter.

4. $S_{s_j s_k}(f) =$ the power cross-spectral density of the outputs of the $j\underline{th}$ and $k\underline{th}$ subarray transmitters. This is the Fourier transform of

$$R_{s_j s_k}(\tau) = <E\{s_j(u;t+\tau)s_k^*(u,t)\}>$$

We expect these to definitely be nonzero since all subarray transmitters are transponding the same pilot tone with basically the same modulation on it.

We further assume that for purposes of this spectral computation we can set the carrier tracking phase $\theta(u,t)$ to a constant $\theta(u)$.

Now it is a simple matter to compute the power spectral density of the interference at the input to the second IF filter, due to these signals. The resultant equivalent baseband power spectral density is:

$$S_{m_I}(f) = S_{c_R}(f) * \left\{ |G_1(f)|^2 \left[(2N_0 + S_{m_{RFI}}(f)) |G_{RF}(f)|^2 \right. \right.$$
$$\left. \left. + \sum_{i=1}^{N} \sum_{k=1}^{N} S_{m_i m_k}(f) G_{ij}(f) G^*_{kj}(f) \right] \right\}$$

where

$$S_{m_{RFI}}(f) = 4U(f+f_0)S_{RFI}(f+f_0)$$

$$S_{m_i m_k}(f) = 4U(f+f_0)S_{s_i s_k}(f+f_0), \quad i \neq k$$

$$G_{ij}(f) = U(f+f_0)H_{ij}(f+f_0)$$

and

$$S_{m_i m_i}(f) = 4U(f+f_0)S_{s_i}(f+f_0)$$

The function $S_{c_R}(f)$ represents the power spectral density of the
PN code reference signal generated in the receiver.

3.3 Intelligent Jamming

In this situation the jammer attempts to emulate the pilot tone,
either to add narrowband noise modulation and jam the data signal, or
to beam steal. To be effective in either case, the jammer must
initially synchronize his SS code modulation with the pilot tones
SS code modulation so that they arrive nearly in phase at the
receiver. He must also deliver a signal power level at least
comparable to the pilot signal's level at the spacetennas subarray
terminals. The basic power density analysis is similar to that used
for the pilot signal earlier.

4. DESIGNING THE FIRST IF FILTER

In this portion of the design it seems reasonable to assume that
the unintentional RFI and the intelligent jamming signals are not
present. The SS processing (code multiplier and second IF filter)
is the key to rejecting these interference signals. The major
purpose of the first IF filter is to reject as much of the extremely
strong downlink signal as is possible.

One plausible criterion for the design of $H_1(f)$ or its baseband
equivalent $G_1(f)$ is to maximize the signal-to-interference density
ratio SIDR in the center of the second IF filter passband. Thus we
consider

$$SIDR = \left. \frac{E\{|P_0(u)|^2\}S_B(f) * S_d(f)}{S_{c_R}(f) * [|G_1(f)|^2 S_I(f)]} \right|_{f=0}$$

where

$$P_0(u) = \frac{1}{T_c} \int_{-T_c/2}^{T_c/2} P(t)Q(t-e(u))dt$$

which by Parsevals theorem is

$$P_0(u) = \frac{1}{T_c} \int_{-\infty}^{\infty} |p(f)|^2 G_{RF}(f)e^{-j\omega e(u)}G_1(f)df$$

with $p(f)$ being the Fourier transform of $P(t)$. Also the quantity $S_I(f)^*$ in the denominator is given by

$$S_I(f) = 2N_0|G_{RF}(f)|^2 + \sum_{i=1}^{N} \sum_{k=1}^{N} S_{m_i m_k}(f)G_{ij}(f)G_{kj}^*(f)$$

Another plausible criterion for the design of the first IF filter is the maximization of the signal-to-interference power ratio in the passband of the second IF filter.

$$SIPR = \frac{E\{|P_0(u)|^2\}\int_{-\infty}^{\infty} |G_2(f)|^2[S_B(f) * S_d(f)]df}{\int_{-\infty}^{\infty} |G_2(f)|^2(S_{c_R}(f) * [|G_1(f)|^2 S_I(f)])df}$$

The problem with both of these performance measures is their dependence on parameters which are not decided at this point.

Before continuing we must get an idea of the shape of $S_{c_R}(f)$. Its spectral density is computed in Appendix 4. Below is a sketch of the envelope of the line spectrum $S_{c_R}(f)$ assuming that the spectrum $S_a(n)$ of the sequence $\{a_n\}$ is flat (see Appendix 4 for definitions.)

$S_{c_R}(f)$

Envelope of Line Powers in $S_{c_R}(f)$. Line Spacing=$1/MT_c$. M = Period of $\{a_n\}$.

$$-\frac{4}{T_c} \qquad -\frac{2}{T_c} \qquad 0 \qquad \frac{2}{T_c} \qquad \frac{4}{T_c}$$
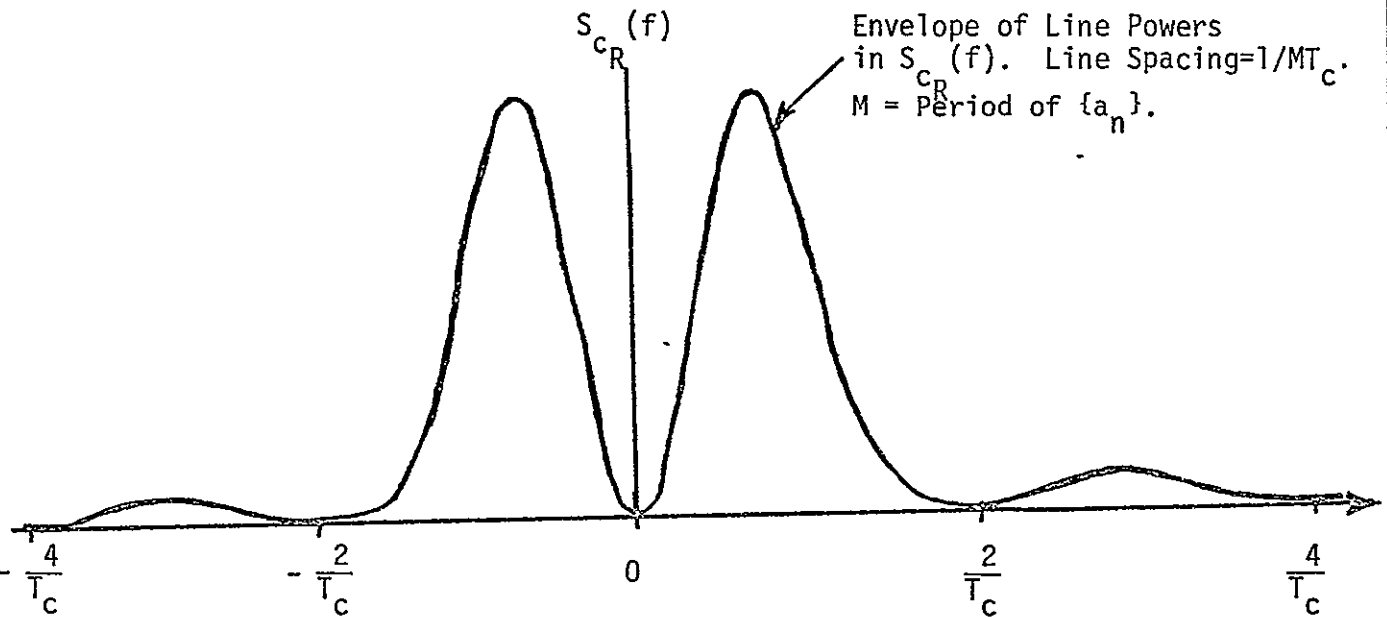
When the line spacing $1/MT_c$ in $S_{c_R}(f)$ is much less than the width of $S_I(f)$, and assume $S_a(f)$ is flat, we can approximate

$$S_{c_R}(f)*[|G_1(f)|^2 S_I(f)]\Big|_{f=0} \quad ,$$

$$\sim \text{constant} \times \int_{-\infty}^{\infty} |p(f)G_1(f)|^2 S_I(f)df$$

and hence

$$\text{SIDR} \sim \text{constant} \times \frac{E\left\{\left|\int_{-\infty}^{\infty} |p(f)|^2 G_{RF}(f)e^{-j\omega e(u)} G_1(f)df\right|^2\right\}}{\int_{-\infty}^{\infty} |p(f)G_1(f)|^2 S_I(f)df}$$

In many SS systems, the line spacing $1/MT_c$ is also the data bandwidth and the approximate bandwidth of the $2\underline{\text{nd}}$ IF filter. In this case we make the approximation

$$\int_{-\infty}^{\infty} |G_2(f)|^2 S_{c_R}(f-\alpha)df$$

$$\sim \text{constant} \times |p(\alpha)|^2$$

where $|p(f)|^2$ is the envelope of the line spectrum $S_{c_R}(f)$, and again we assumed $S_a(n)$ is flat. This can be used to significantly simplify the denominator of SIPR, and

$$\text{SIPR} \sim \text{constant} \times \frac{E\left\{\left|\int_{-\infty}^{\infty} |p(f)|^2 G_{RF}(f)e^{-j\omega e(u)}G_1(f)df\right|^2\right\}}{\int_{-\infty}^{\infty} |p(f)G_1(f)|^2 S_I(f)df}$$

So under certain circumstances both SIPR and SIDR have approximately the same dependence on $G_1(f)$ shown explicitly above.

Lets work on the numerator expression to evaluate the expected value and determine its relation to the denominator.

$$\text{Numerator} = \iint_{-\infty}^{\infty} |p(f_1)|^2 G_{RF}^*(f_1)G_1^*(f_1)|p(f_2)|^2 G_{RF}(f_2)G_1(f_2)$$
$$E\{e^{j(\omega_1-\omega_2)e(u)}\}df_1 df_2$$

To continue precisely much depends on the characteristic function of the tracking error. The integrals factor only if we assume $e(u) \approx E\{e(u)\} = m_e$, i.e. $e(u)$ is very close to its mean value with probability approaching one. Lets assume this is true and see what happens:

$$\text{Numerator} = \left|\int_{-\infty}^{\infty} |p(f)|^2 G_{RF}(f)G_1(f)e^{-j\omega m_e}df\right|^2$$

Applying Schwartz's inequality then gives

$$\text{Numerator} \leq \int_{-\infty}^{\infty} |G_1(f)p(f)\sqrt{S_I(f)}|^2 df$$
$$\times \int_{-\infty}^{\infty} \left|\frac{1}{\sqrt{S_I(f)}} G_{RF}(f)p^*(f)e^{-j\omega m_e}\right|^2 df$$

or

$$\frac{\text{Numerator}}{\text{Denominator}} \leq \int_{-\infty}^{\infty} \frac{|G_{RF}(f)p(f)|^2}{S_I(f)} \, df \sim \text{SIDR}_{max} \text{ or } \text{SIPR}_{max}$$

The maximum on the right is independent of $G_1(f)$ and is achieved when

$$G_1(f) \approx \frac{G_{RF}^*(f)e^{j\omega m_e}}{S_I(f)}$$

We must now try to design a decent approximation to $G_1(f)$, even though it may be difficult to approximate m_e and determine $S_I(f)$ precisely.

5.0 APPROXIMATIONS TO THE INTERFERENCE SPECTRUM $S_I(f)$

The major problem encountered in attempting the design of $H_1(f)$ (or the equivalent $G_1(f)$) is the evaluation of $S_I(f)$. Recall that

$$S_I(f) = 2N_0|G_{RF}(f)|^2 + \sum_i \sum_k S_{m_i m_k}(f)G_{ij}(f)G_{kj}^*(f)$$

represents the equivalent baseband power spectral density of the interference at the RF output of spacetenna receiver j. Hopefully hardware experience will provide us with estimates of $N_0/2$ and $G_{RF}(f)$. The complicated double sum however requires some simplification.

We shall write the following expression for the signal transmitted by the $k\underline{\text{th}}$ antenna subarray.

$$s_k(t) = \text{Re}\{m_k(u,t)e^{j\omega_c t}\}$$

where

$$m_k(u,t) = A_k(u,t)e^{j[\phi(u,t-d_k)+\omega_c d_k]}$$

d_k = The differential delay between the pilot tone arrival at subarray k and the pilot tone arrival at subarray j.

$\phi(u,t)$ = The phase function appearing on the output of the $j\underline{th}$ subarray transmitter in the absence of transmitter noise and receiver noise. The time variations in $\phi(u,t)$ are due to the modulation factor $a(u,t)b(u,t)$ on the pilot tone.

$\omega_c d_k$ = Differential carrier phase shift between the pilot tone at subarray k and the pilot tone at subarray j.

$A_k(u,t)$ = Effects of transmitter and receiver noise generated in subarray k.

Ideally $A_k(u,t) = a_0$ for all k, and $m_k(u,t)$ would be the same as $m_j(u,t)$ except for a time delay and a constant complex phase factor.

We now make the following assumptions:

(a) $\{A_k(u,t)\}$ is a set of independent, identically-distributed wide-sense stationary random processes each with mean $\overline{A}$ and covariance $K_A(\tau)$.

$$E\{A_k(u,t)\} = \overline{A}, \qquad \forall k,t .$$

$$\text{Cov}\{A_k(u,t_1)A_k(u,t_2)\} = K_A(t_1-t_2), \quad \forall k,t_1,t_2 .$$

(b) $\phi(u,t)$ is a stationary random process with the function

$$E\{\exp(j[\phi(u,t+\tau)-\phi(u,t)])\} = \Phi(\tau)$$

known.

(c) $\{A_k(u,t)\}$ and $\phi(u,t)$ are independent random processes.

Under these assumptions it is easily shown that

$$R_{m_j m_k}(t_1,t_2) \triangleq E\{m_j(u,t_1)m_k(u,t_2)\}$$

$$= \begin{cases} \overline{A}^2\Phi(t_1-t_2-d_j+d_k)e^{j\omega_c(d_j-d_k)}, & i\neq k \\[2ex] [K_A(t_1-t_2)+\overline{A}^2]\Phi(t_1-t_2), & i=k \end{cases}$$

Defining Fourier transforms

$$S_{m_i m_k}(f) = \int_{-\infty}^{\infty} R_{m_i m_k}(\tau) e^{-j2\pi f \tau} d\tau$$

$$S_{\phi}(f) = \int_{-\infty}^{\infty} \Phi(\tau) e^{-j2\pi f \tau} d\tau$$

$$S_A(f) = \int_{-\infty}^{\infty} K_A(\tau) e^{-j2\pi f \tau} d\tau,$$

It follows that

$$S_{m_i m_k}(f) = \begin{cases} \overline{A}^2 S_{\phi}(f) e^{j2\pi(f_c - f)(d_i - d_k)}, & i \neq k \\ [\overline{A}^2 \delta(f) + S_A(f)] * S_{\phi}(f), & i = k \end{cases}$$

This can now be used to simplify the expression for the inter-
ference power spectral density at the RF terminals of the $j^{\underline{th}}$
subarray receiver,

$$S_I(f) = 2N_0 |G_{RF}(f)|^2 + [S_A(f) * S_{\phi}(f)] \sum_{k=1}^{N} |G_{kj}(f)|^2$$

$$+ \overline{A}^2 S_{\phi}(f) \left| \sum_{k=1}^{N} G_{kj}(f) e^{j2\pi d_k (f_c - f)} \right|^2$$

This has considerably simplified the requirements for power spectral
density information, and indicates the precise dependence of the
interference power spectral density on the baseband equivalent RF
system functions and on the pilot signals direction of arrival (which
is hidden in $\{d_k\}$).

6.0 DESIGN PARAMETERS AND CONSTANTS

The preceding sections provide a mathematical framework in which to study the interference rejection problem. We will now choose some design parameters and design constants for use in later computations:

(a) Thermal Noise Density:

$$N_0 = kT = .69 \times 10^{-20}$$

Here k is Boltzmann's Constant and T is 500°K.

(b) Spacetenna Subarray Transmitter Noise Characteristics:

$$\overline{A} = {}^{'}\sqrt{2P}\, e^{-\sigma_\theta^2}$$

$$, S_A(f) = 4Pe^{-2\sigma_\theta^2}\alpha S_0(f)$$

where

P = Transmitter Power = 65 kw

σ_ϑ^2 = Transmitter Phase Error Variance

$= .0305\ rad^2 \sim (10°\ rms)$

α = Variance to-squared-mean ratio of the angular modulation

$\approx \sigma_\theta^2$

$S_0(f)$ = normalized phase error spectral density

$$= \begin{cases} c\ , & |f| < 1\ KHz \\ c(f/10^3)^{-6}\ , & 1\ KHz < |f| < 10\ KHz \\ c\ 10^{-6}(f/10^4)^{-2}, & 10\ KHz < |f| \end{cases}$$

c = normalizing constant = $(2.4 \times 10^3)^{-1}$

The development of the model for subarray transmitter noise is discussed in Appendix V. $S_A(f)$ in dB above 1 W/Hz is shown in Figure 6.1.

79-0259

Figure 6.1. A Plot of the Assumed Power Density $S_A(f)$.

46 0700

10 X 10 TO THE INCH • 7 X 10 INCHES
KEUFFEL & ESSER CO   MADE IN USA
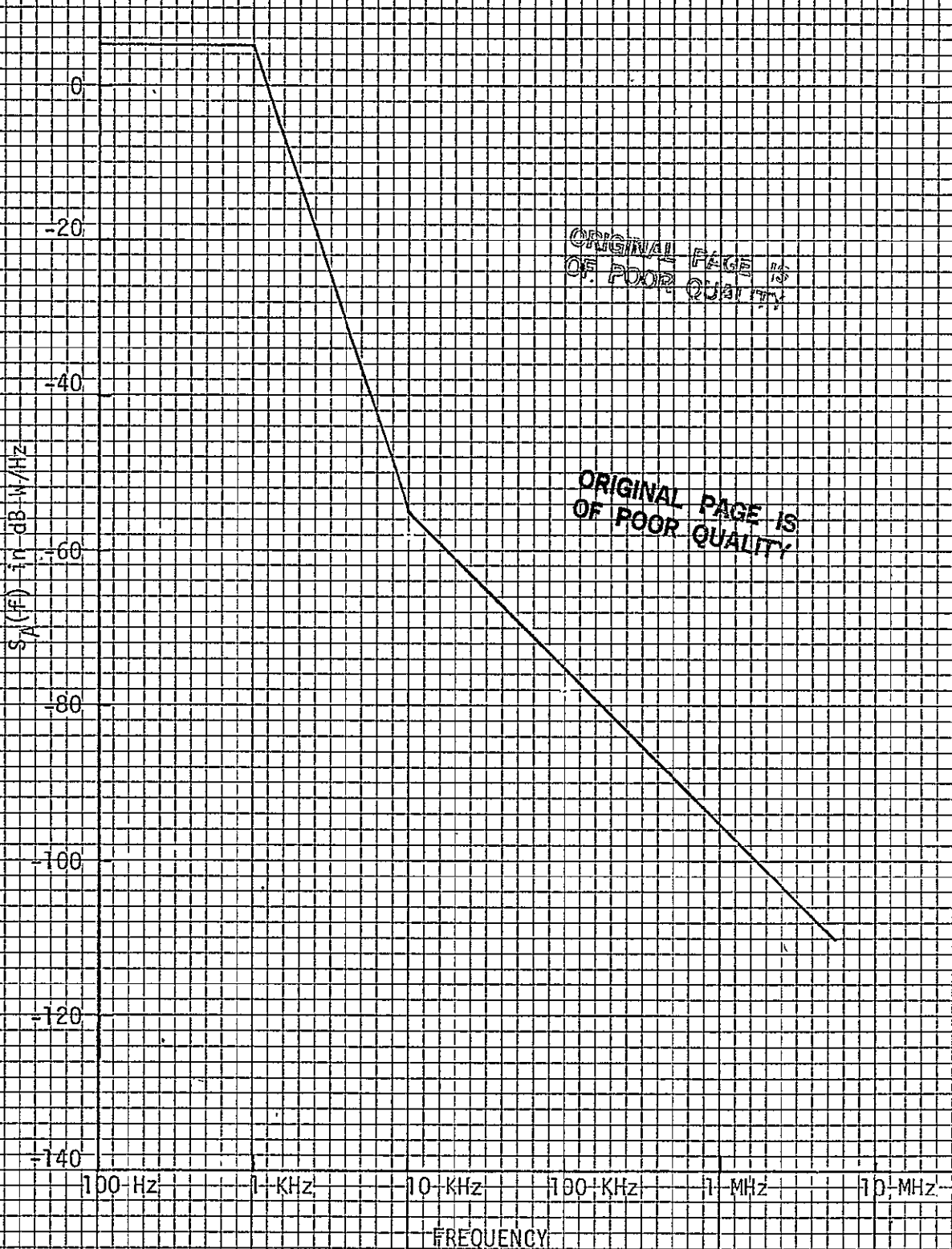
ORIGINAL PAGE IS
OF POOR QUALITY

$S_A(f)$ in dB-W/Hz

FREQUENCY

-29-

(c) Spectral density of spurious phase modulation on the uplink signal:

$$S_\phi(f) = \delta_D(f) \text{ (Dirac Delta Function)}$$

This is a reasonable approximation for interference computations.

(d) Chip rate:

$$T_c = 10^{-7} \text{ sec}$$

(e) Baseband-equivalent RF filter:

$$G_{RF}(f) = \frac{1}{1+j2\pi f\tau}$$

The time constant τ of this filter is normalized in terms of chip times to

$$\alpha \triangleq \frac{\tau}{T_c}$$

Note the 3 dB cutoff point for $G_{RF}(f)$ is $\frac{1}{2\pi\tau}$. Figure 6.2 is a sketch of $|G_{RF}(f)|^2$. The one-pole Butterworth filter characteristic has been chosen to conform with frequency response of half module radiator supplied by Boeing. A comparison is given in Fig. 6.3.

(f) The noncoherent-interference-coupling equivalent-baseband system function:

$$\sum_k |G_{kj}(f)|^2 \leq K_1' \text{ (constant)}$$
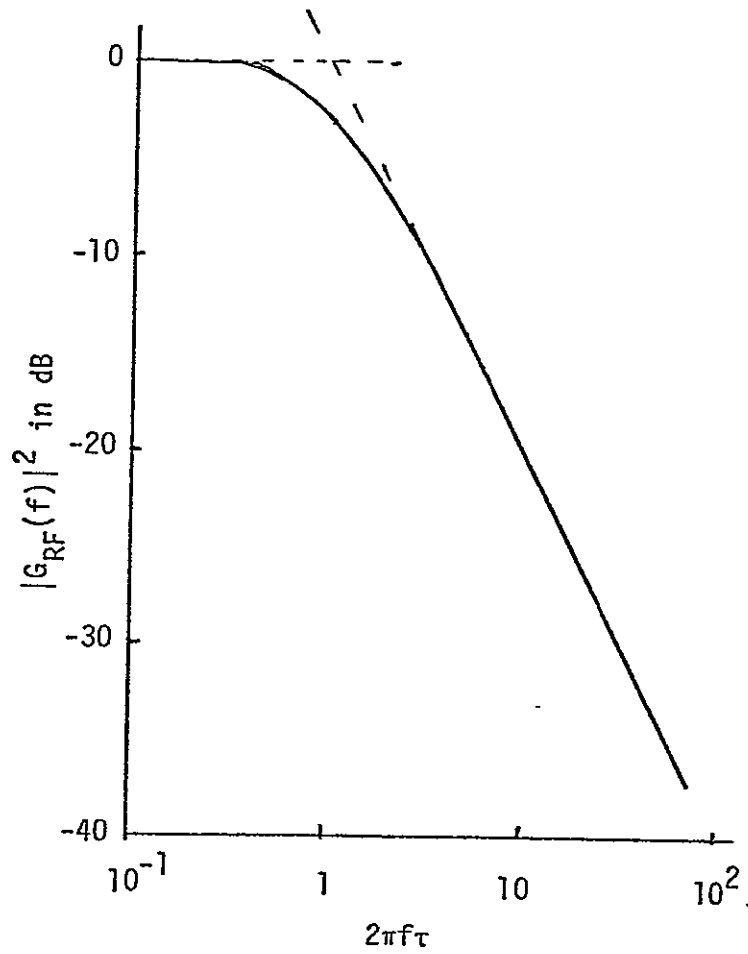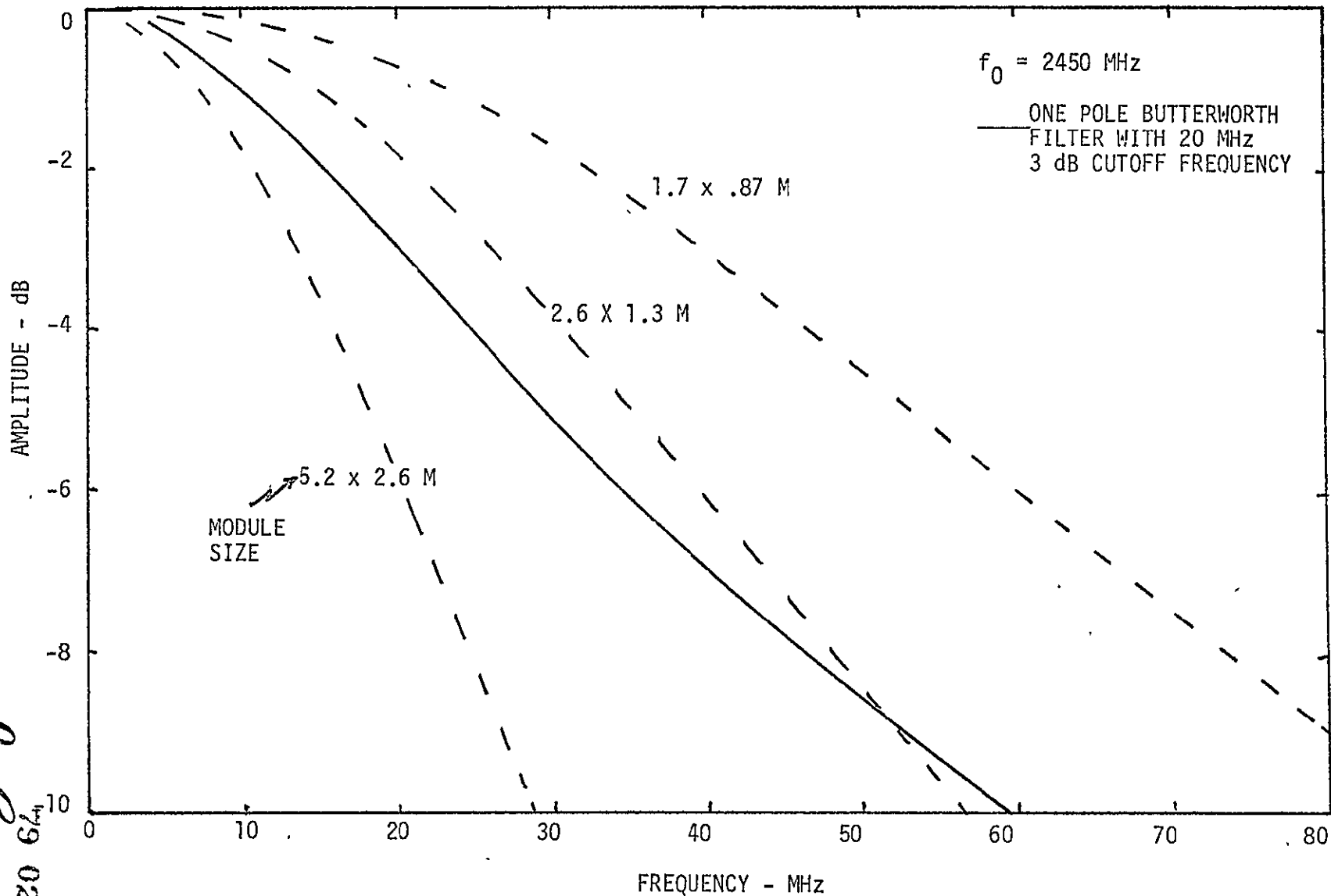
Here K_1 is an array design parameter.

Figure 6.2. The Assumed Power Response of the RF Filter.

Figure 6.3. Frequency Response of Half Module Radiator.

(g) The coherent-interference-coupling equivalent-baseband system function:

$$\left| \sum_k G_{kj}(f) e^{j2\pi d_k(f_c - f)} \right|^2 \leq K_2 \quad \text{(A Constant)}$$

Here K_2 is an array design parameter.

(h) The PN apparent tracking offset e is normalized in terms of chip times.

$$\beta \overset{\Delta}{=} \frac{e}{T_c}$$

(i) The first IF filter in equivalent baseband form is given by

$$G_1(f) = \gamma + \prod_{n=3}^{8} \frac{1}{(\frac{f_0}{jf}) - \exp(j(2n+1)\pi/12)}$$

This is a high-pass Butterworth filter with an added constant γ which can be used to specify the quality of the filter's null at bandcenter. Six poles were chosen since this matches the predicted theoretically optimal filter (see Section 4) in the critical range where $S_A(f)$ has a 60 dB per decade slope. The inversion frequency f_0 is a design parameter. A sketch of $|G_1(f)|^2$ is shown in Figure 6.4.

We also normalize f_0 to the chip rate by defining

$$\delta = f_0 T_c$$

(j) Bi-ϕ Manchester waveform characterization:

Figure 6.4. Power Response of the Assumed First IF Filter.

79 0262

-34-

$P_\varepsilon(t)$ = imperfect Manchester pulse

$$= \begin{cases} \dfrac{1+\varepsilon}{\sqrt{1+\varepsilon^2}} & , \quad -\dfrac{T_c}{2} < t < 0 \\[3mm] \dfrac{-1+\varepsilon}{\sqrt{1+\varepsilon^2}} & , \quad 0 < t < \dfrac{T_c}{2} \\[3mm] 0 & , \qquad \text{otherwise} \end{cases}$$

$$= \frac{1}{\sqrt{1+\varepsilon^2}} P(t) + \frac{\varepsilon}{\sqrt{1+\varepsilon^2}} |P(t)|$$

Hence $P_\varepsilon(t)$ is a weighted sum of the Manchester waveform $P(t)$ and the NRZ waveform $|P(t)|$, (see Fig.6.5).

The squared-magnitude of the Fourier transform of $P_\varepsilon(t)$, after normalization, is given by

$$\left| \frac{P_\varepsilon(f)}{T_c} \right|^2 = \frac{1}{1+\varepsilon^2} \frac{\sin^4(\pi f T_c/2)}{(\pi f T_c/2)^2} + \frac{\varepsilon^2}{1+\varepsilon^2} \frac{\sin^2(\pi f T_c)}{(\pi f T_c)^2}$$

which is a linear combination of the energy spectrum of the Manchester waveform and the energy spectrum of the NRZ waveform.

$P_\varepsilon(t)$ and $p_\varepsilon(f)$ will replace $P(t)$ and $p(f)$ in some of the equations derived earlier so that we can estimate the effects of an imperfect PN code waveform on the leakage of narrowband interference into the passband of the second IF filter. Thus ε is a basic design parameter.

$$\frac{1+\epsilon}{\sqrt{1+\epsilon^2}}$$

$$\frac{-1+\epsilon}{\sqrt{1+\epsilon^2}}$$

$-T_c/2$

$T_c/2$

$-T_c/2$

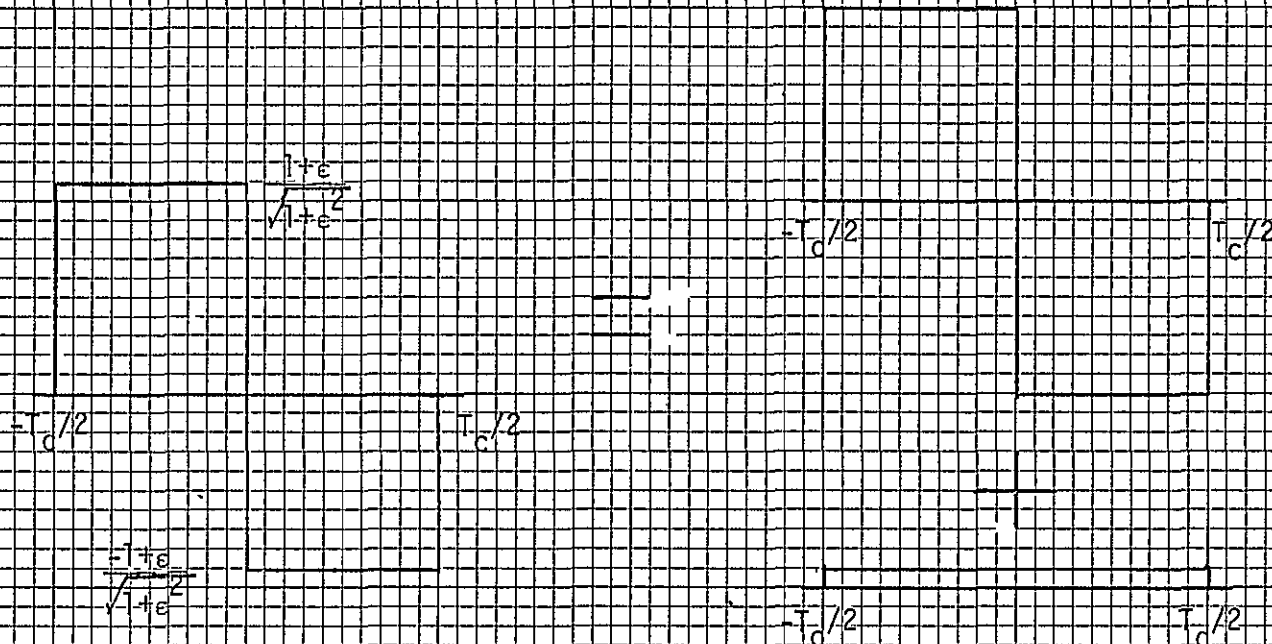$T_c/2$

$-T_c/2$

$T_c/2$

Figure 6.5. Model for PN Chip Asymmetry.

LinCom

7.0 INTERFERENCE LEVELS AT THE OUTPUT OF THE SECOND IF FILTER

Under the assumptions of the previous section, the interference spectral density in the worst case is given by

$$S_I(f) = 2N_0|G_{RF}(f)|^2 + K_1 S_A(f) + K_2 \bar{A}^2 \delta_D(f)$$

Using this as our model for $S_I(f)$, we can evaluate the effect of the notch filter parameters f_0 and γ on the interference power I_F at the output of the first IF filter.

$$I_F = \int_{-\infty}^{\infty} S_I(f)|G_1(f)|^2 df$$

The results of this computation are given in Table 7-1, along with a breakdown of the contributions to I_F of the three components of $S_I(f)$, namely thermal noise, noncoherent downlink interference, and coherent downlink interference. The width f_0 of the notch filter is limited by the loss of uplink signal power which it causes. This will be evaluated in the next section. The minimum value of γ is limited by hardware implementation problems.

The effect of the PN code multiplier in the receiver is to spread the interference power spectrum over a wide band. The power spectral density of the input to the baseband equivalent second IF filter $G_2(f)$ is given by

$$S_{I2IN}(f) = S_{C_R}(f)*[|G_1(f)|^2 S_I(f)]$$

where for an m-sequence, the code spectral density consists of lines $1/MT_c$ apart with:

$$S_{C_R}(f) = \sum_n P_n \delta_D(f - \frac{n}{MT_c})$$

LinCom

-37-

Table 7-1. Effect of Notch Filter Parameters On Interference Level Before PN Despread.

(a) Effect of Cutoff Frequency

$$\gamma = 10^{-3}, \; \beta = 0, \; \alpha = \frac{1}{4\pi}, \; K_1 = K_2 = 10^{-2}, \; T_c = 10^{-7}$$

f_0	I_F	COMPONENTS OF I_F		
		THERMAL	NONCOHERENT	COHERENT
10^2	6.94(1)	7.83(-13)	6.94(1)	1.22(-3)
10^3	1.35(1)	7.83(-13)	1.35(1)	1.22(-3)
5×10^3	7.10(-3)	7.82(-13)	5.88(-3)	1.22(-3)
10^4	1.90(-3)	7.82(-13)	6.78(-4)	1.22(-3)
10^5	1.30(-3)	7.80(-13)	7.57(-5)	1.22(-3)
10^6	1.30(-3)	7.54(-13)	7.57(-5)	1.22(-3)
2×10^6	1.30(-3)	7.26(-13)	7.57(-5)	1.22(-3)
3×10^6	1.30(-3)	6.99(-13)	7.57(-5)	1.22(-3)

(b) Effect of DC Attenuation with Narrowband Notch Filter

$$f_0 = 10^4, \; \beta = 0, \; \alpha = \frac{1}{4\pi}, \; K_1 = K_2 = 10^{-2}, \; T_c = 10^{-7}$$

γ	I_F	COMPONENTS OF I_F		
		THERMAL	NONCOHERENT	COHERENT
10^{-2}	1.30(-1)	7.96(-13)	7.57(-3)	1.22(-1)
10^{-3}	1.90(-3)	7.82(-13)	6.78(-4)	1.22(-3)
10^{-4}	6.17(-4)	7.81(-13)	6.05(-4)	1.22(-5)
10^{-5}	6.04(-4)	7.81(-13)	6.04(-4)	1.22(-7)

(c) Effect of DC Attenuation with Wideband Notch Filter

$$f_0 = 2 \times 10^6, \; \beta = 0, \; \alpha = \frac{1}{4\pi}, \; K_1 = K_2 = 10^{-2}, \; T_c = 10^{-7}$$

γ	I_F	COMPONENTS OF I_F		
		THERMAL	NONCOHERENT	COHERENT
10^{-2}	1.30(-1)	7.36(-13)	7.57(-3)	1.22(-1)
10^{-3}	1.30(-3)	7.26(-13)	7.57(-5)	1.22(-3)
10^{-4}	1.30(-5)	7.26(-13)	7.57(-7)	1.22(-5)
10^{-5}	1.30(-7)	7.25(-13)	7.57(-9)	1.22(-7)

where

$$P_n = \begin{cases} \dfrac{1}{M^2} \left| \dfrac{P_\varepsilon(0)}{T_c} \right|^2 & , \; n = 0 \\[2em] \dfrac{1}{M}\left(1+\dfrac{1}{M}\right) \left| \dfrac{P_\varepsilon(\frac{n}{MT_c})}{T_c} \right|^2 & , \; n \neq 0. \end{cases}$$

Hence the resultant spectral density at the input to the baseband-equivalent second IF filter contains lines separated by $\frac{1}{MT_c}$ hertz along with a continuous spectral density. We assume that the second IF filter has a bandwidth narrow enough to reject all lines except the center line in $S_{I2IN}(f)$. For example let's assume that $G_2(f)$ is a zonal filter:

$$G_2(f) = \begin{cases} 1 & , \quad |f| < \dfrac{1}{2MT_c} \\[1em] 0 & , \quad \text{otherwise}. \end{cases}$$

This idealistic assumption is not critical since a "narrower" non-ideal filters occur in the carrier tracking loops which follow. Then we approximate the output baseband equivalent second IF filter by:

$$S_{I2OUT}(f) = 2N_{eq} + 2J\delta_D(f) , \quad |f| < \frac{1}{2MT_c}$$

where $2N_{eq}$ is the continuous spectral density at band center, and J is the d.c. line power,

$$2N_{eq} = \sum_n P_n \left| G_1\left(\frac{n}{MT_c}\right) \right|^2 \left[2N_0 \left| G_{RF}\left(\frac{n}{MT_c}\right) \right|^2 + K_1 S_A\left(\frac{n}{MT_c}\right) \right] ,$$

$$2J = \gamma^2 P_0 K_2 \overline{A}^2$$

Notice that if $P_\varepsilon(t)$ is a perfect Manchester pulse, i.e., $\varepsilon = 0$, then $J = 0$ and the line in this density disappears, implying that in this case the interference can be made proportionately smaller by decreasing

the loop bandwidth.

The spectral density $S_{I2OUT}(f)$ which we have just developed is the spectral density of the complex valued modulation on the IF signal at the output of $H_2(f)$. The spectral density of the actual IF signal at the output of $H_2(f)$ is given by

$$S_{S_{I}2OUT}(f) = \begin{cases} \dfrac{N_{eq}}{2} + \dfrac{J}{2}\,[\delta(f-f_{IF}) + \delta(f+f_{IF})], & |f \pm f_{IF}| < \dfrac{1}{2MT_c} \\[2em] 0, & \text{otherwise} \end{cases}$$

This expression will be used in later sections to determine tracking loop signal-to-noise ratios. The effect of the code length M on the noise process is shown in Table 7-2.

8.0 UPLINK SIGNAL LEVELS AT THE OUTPUT OF THE SECOND IF FILTER

The uplink pilot signal power P_R at the terminals of the subarray antenna is given by

$$P_R = \frac{P_T G_T A_R}{4\pi R^2}$$

where

P_T = Pilot transmitter power = 65 kw

$G_T = \eta\,\dfrac{4\pi A_T}{\lambda^2}$ = Pilot Antenna Gain $\doteq$ 32,900

λ = Pilot transmitter wavelength = .12245m

A_T = Pilot antenna aperture area = 78.5 m^2 (10m dish)

η = Transmit efficiency = .5

A_R = Subarray pilot antenna perture = 3m^2

R = range = 38,000 km

Table 7-2. Effect of Code Length M on Equivalent Noise Seen by Costas Loop.

M	N_{eq}	J
1	2.6(-15)	6.12(-6)
2	4.9(-15)	1.53(-6)
3	5.3(-14)	6.79(-7)
4	5.2(-14)	3.82(-7)
10	5.2(-14)	6.12(-8)
100	5.2(-14)	6.12(-10)
1,000	5.2(-14)	6.12(-12)
10,000	5.2(-14)	6.12(-14)

$$K_1 = K_2 = 10^{-2}$$

$$T_c = 10^{-7}$$

$$\gamma = 10^{-3}$$

$$\alpha = \frac{1}{4\pi}$$

$$\delta = 10^{-3}$$

$$\varepsilon = 10\%$$

The received pilot signal power then is

$$P_R \doteq .354 \; \mu W.$$

As discussed in Section 3.1, the pilot signal undergoes a fractional gain due to the notch in the first IF filter and to RF filtering, which is given by

$$L_F = \left| \frac{1}{T_c} \int_{-\infty}^{\infty} |P_\varepsilon(f)|^2 G_{RF}(f) G_1(f) e^{-j2\pi f \varepsilon} df \right|^2$$

where ε is the PN apparent tracking offset. Figure 8-1 indicates the variation in L_F as the normalized PN apparent tracking offset β varies between ± 1 chip time. Notice that in the most optimistic case for the chosen parameters, L_F is less than 0.7 and that tracking error from this maximum must be on the order of 0.1 T_c to keep L_F above 0.6. Our nominal choice of $\beta = 0$ for later power computations puts L_F at about 0.55. The fractional power loss is also function of the RF terminal response $G_{RF}(f)$ and the notch filter $G_1(f)$. The results are given in Table 8-1. For these tables, we have also indicated the loss if phase compensation for the filters ($G_{RF}(f)$ and $G_1(f)$) are used.

We assume that the carrier tracking loop is operating properly and that a nominal unit gain is seen by the pilot signal's center-line when passing through the second IF filter.

9.0 COSTAS LOOP PHASE ERROR

At the input to the Costas loop, the signal consists of three terms: a term due to the uplink pilot data modulation with power $P_R \cdot L_F$, a line due to the interference with power J and an equivalent "white" noise term with one-sided spectral density N_{eq}. From [7], the phase error of a Costas loop is given by

SIGNAL POWER LOSS, L_F

$\alpha = 1/4\pi$

$\gamma = 10^{-3}$

——— $\delta = 10^{-3}$

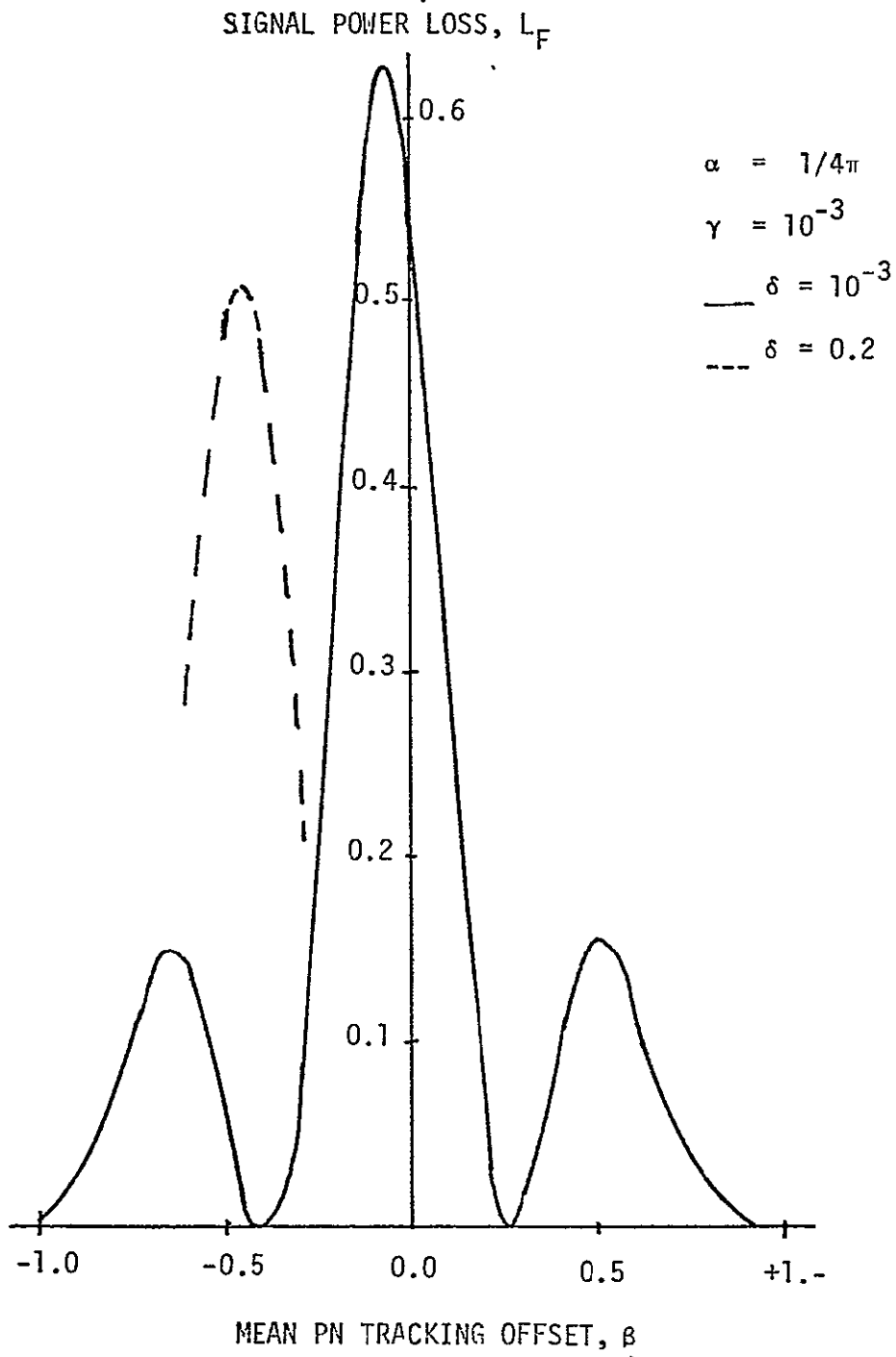- - - $\delta = 0.2$

MEAN PN TRACKING OFFSET, β

Figure 8.1. Pilot Signal Power Gain Through the Receiver as a
Function of PN Apparent Tracking Offset.

Table 8-1. Effect of $G_{RF}(f)$ and Notch Filter Bandwidth on Fraction Power Loss L_F.

(a) Effect of Notch Filter

δ	L_F (peak)	L_F^*
10^{-3}	.63	.63
10^{-2}	.63	.63
10^{-1}	.63	.63
.2	.51	.61
.4	.35	.51
.6	.29	.35
.8	.15	.18

$T_c = 10^{-7}$

$\gamma = .001$

$\alpha = 1/4\pi$

(b) Effect of RF Terminal Response $G_{RF}(f)$

$(2\pi\alpha)^{-1}$	L_F^*
.2	.06
.5	.25
1	.49
2	.72
5	.88
10	.93
20	.96
50	.97

$T_c = 10^{-7}$

$\gamma = 10^{-3}$

$\delta = 10^{-1}$

*With ideal phase compensation.

$$\sigma_\phi^2 = \mathcal{S}_L^{-1} \frac{N_{eq}B_L}{P_R \cdot L_F}$$

where B_L is the one-sided loop bandwidth and $\mathcal{S}_L$ is the squaring loss which is a function of the IF filter and the arm filters. A typical squaring loss is 2 dB. The interference term will also introduce a phase error which depends on J and the random phase between the interference and the carrier. We shall adopt a worst case analysis, i.e., the carrier and the interference are at quadrature with each other. The phase error is now modified to

$$\sigma_\phi^2 = \mathcal{S}_L^{-1} \frac{N_{eq}B_L}{P_R \cdot L_F} + \frac{J}{P_R \cdot L_F}$$

If no data modulation is employed for the uplink pilot, the carrier recovery can be accomplished with a CW loop. In that case, the squaring loss penalty is removed. It also reduces hardware problems such as balancing the I and Q arm filters when a Costas loop is used.

10.0 SPREAD SPECTRUM CODE SELECTION

The system design, as analyzed earlier, depends on the spread spectrum sequence (SSS) $\{a_i\}$ in several ways:

(a) The d.c. line energy in the code spectral density, namely P_0, is the same for any balanced sequence of odd period. Hence we have assumed that the SSS has a number of ones and a number of zeros in one period which differ by 1.

(b) The SSS spectral line spacing is $(MT_c)^{-1}$ hertz and it is assumed that all but the d.c. line would be rejected by the second IF filter. Hence the code period M must satisfy the relation

$$M \ll B_2 T_c$$

where B_2 is the bandwidth of the second IF filter, or the filter must have carefully constructed nulls at multiples of $1/MT_c$.

(c)   The equivalent noise spectral density parameter N_{eq} is a function of the SSS spectral line levels P_n for all n.

(d)   To provide a good characteristic for the code tracking loop, the SSS must have a spike-like periodic autocorrelation function.

Now lets investigate the options open to us under these constraints.

With a chip time of 10^{-7} seconds and a second IF filter bandwidth on the order of 100 hertz, the period of the sequence must be less than 10^4 to satisfy the line rejection constraint (b). Certainly maximum-length linear-feedback shift register sequences, i.e., m-sequences, satisfy the remaining constraints. They are balanced and have spike-like autocorrelation functions. The numerical data for N_{eq} given in Section 7 is based on the values of P_n for m-sequences.

The following gives the number of distinct m-sequences and their period M, as a function of shift register length L, along with a typical shift register generator.

Register Length	Period	Number of Sequences	Typical Generator
9	511	56	9,4
10	1023	99	10,3
11	2047	186	11,1
12	4095	335	12,6,4,1
13	8191	630	13,4,3,1
14	16383	1161	14,12,2,1

To construct the m-sequence from the generator information in the above table, simply take the modulo 2 sum of the outputs of the stages indicated in the table and feed the result back into the shift register. An example is given below for the length 12.

STAGE NUMBER

MODULO 2 ADDERS
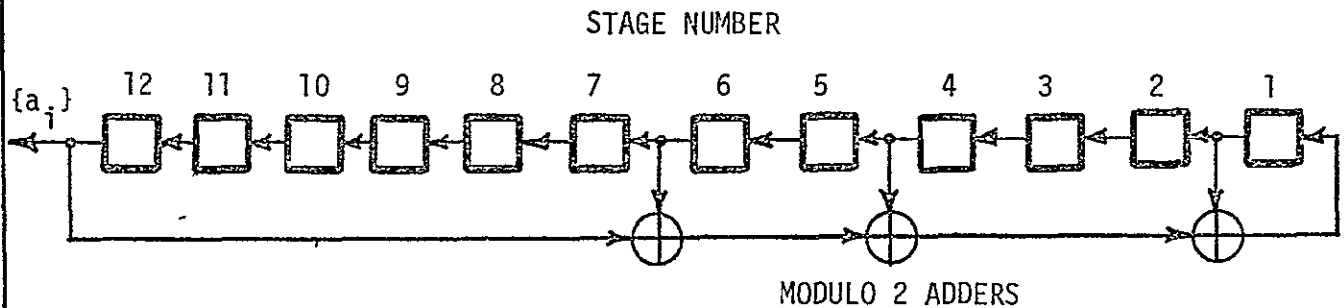
Load the register with any sequence of bits, not all zero, and as it runs it will produce some phase shift of the m-sequence associated with the particular register. Changing to a different seqeunce involves changing the tap connections. Appropriate connections for other generators are determined using a table of primitive polynomials over GF(2), e.g., the table in [3].

If code-division multiple access schemes are required to provide satisfactory isolation betweenthe pilot signals from different rectennas, then there are several alternatives, all based on shift register generated sequences. They are (a) Gold Codes, (b) Kasami Sequences, and (c) Bent-Function Sequences. All are easily implemented. Properties of these sequence sets are tabulated below for designs of period 2^n-1. The Gold Codes are suboptimal from two viewpoints: They are not all balanced, and their crosscorrelation is approximately $\sqrt{2}$ too large. Both Kasami sequences and bent sequences offer an alternative to Gold sequences with better correlation properties. The Kasami sequences

Property	Gold [4]	Kasami [5]	Bent [6]
All Balanced	No	No	Yes
Number of Sequences	2^n+1	$2^{n/2}$	$2^{n/2}$
Allowable n	n not divisible by 4	n even	n a multiple of 4
Maximum Cross-Correlation	$2^{(n/2)+1}+1$, n even $2^{(n+1)/2}+1$, n odd	$2^{n/2}+1$	$2^{n/2}+1$
Linear Recursion Length	$2n+1$	$\frac{3}{2}n+1$	Longer

are available in a greater variety of lengths (2^n-1 for all even n) than

bent sequences, but the bent sequences are guaranteed balanced, and in

addition have two nice properties when an intelligent jammer is trying to

cause trouble. First, the linear span of a bent sequence is quite long

for the shift register length employed. Secondly, it is quite easy in

hardware to reinitialize a given bent sequence to a new random phase.

In the code division multiple access situation, we would recommend

the use of the set of 64 bent function sequences of period 4095. The

design details are available in [6] along with a sample design for n=12.

For a further discussion, see Appendix 6.

11.0 PERFORMANCE EVALUATION VIA SOLARSIM

In the precding sections, analytical models have been developed in terms of the pertinent design parameters of the receiver portion of the SPS transponder. These important parameters include:

- Bi-ϕ Waveform Asymmetry
- PN Chip Rate
- PN Code Period
- Uplink EIRP
- Receiver G/T
- Diplexer Isolation
- RF Path Cutoff Frequency
- Notch Filter Stop Band and Attenuation
- Costas Loop Bandwidth

They serve to characterize the uplink waveform, the link budget, the receiver RF front end, interference nulling IF filter and the phase tracking system. In order to optimally select these parameters, the SOLARSIM has been updated to include a computer program to evaluate the performance of the transponder as a function of these inputs. The performance measure selected is the phase error of the Costas tracking loop. A description of the computer package is included in Appendix 6.

To demonstrate its value as an evaluation tool, we have used the SOLARSIM package to study the effect of (1) cutoff frequency of RF system function, (2) notch filter cutoff frequency, (3) notch filter attenuation and (4) PN code period on the Costas loop tracking phase jitter with the PN chip rate as a variable. For these examples, the nominal conditions are chosen to represent a practical transponder design and they are listed in Table 11-1. The simulation results are

Table 11-1. Nominal Parameters for SOLARSIM Example.

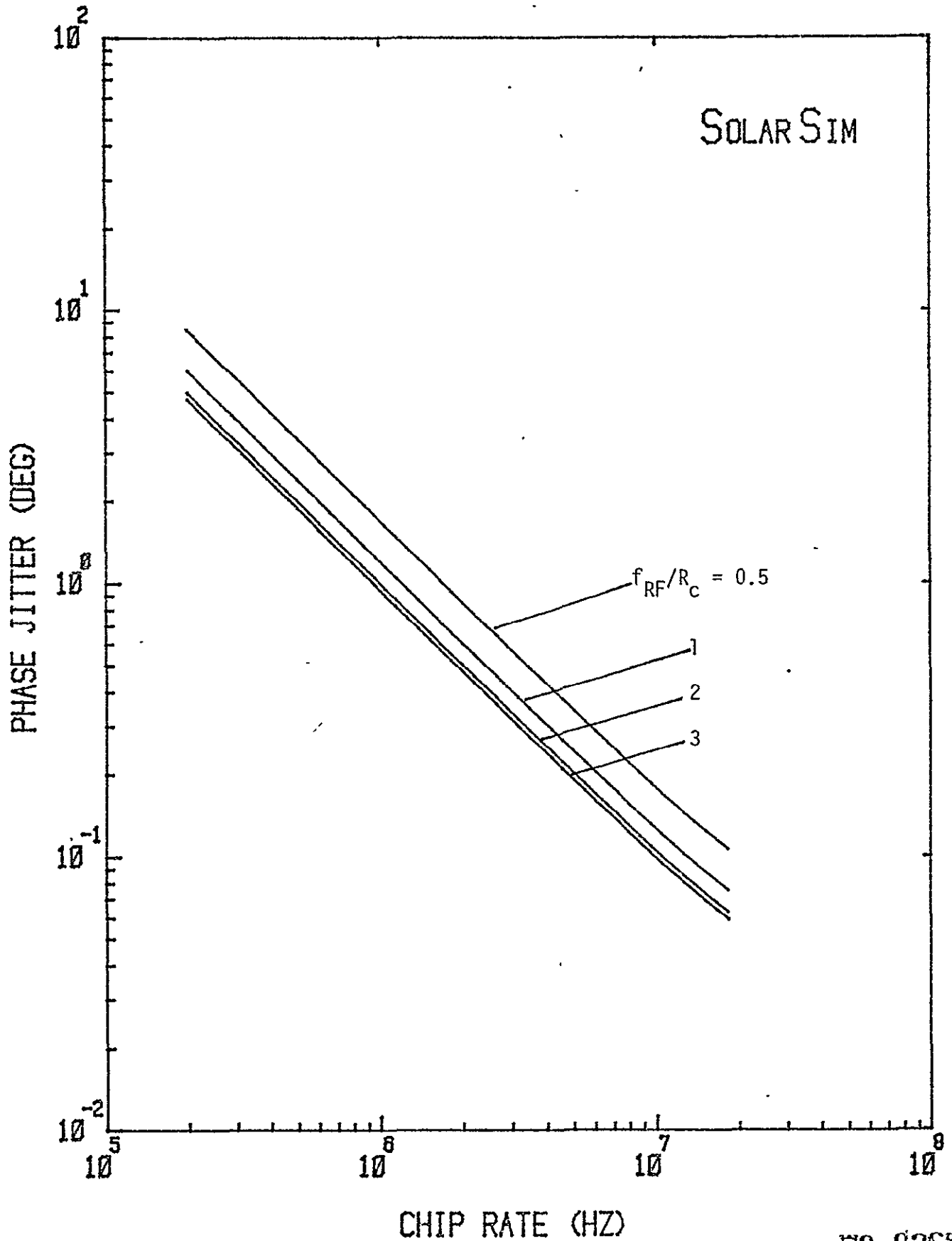| PARAMETER	VALUE
f_{RF}/R_c	2
f_N/R_c	10^{-1}
γ^2	60 dB
e/T_c	At Peak Correlation
K_1	20 dB
K_2	20 dB
M	10^4
ε	10%
B_L	10 Hz
EIRP	93.3 dBW
NF	2.5 dB
A_R	$3m^2$

8

plotted in Figs. 11.1 - 11.5.

Figure 11.1 indicates that widening the RF filter bandwidth relative to the chip rate improves the system performance. However, the improvement margin becomes smaller as f_{RF}/R_c (f_{RF} is the 3 dB cutoff frequency) increases, indicating there is a region of diminishing return beyond $f_{RF}/R_c = 2$. This is to be expected since most of the pilot signal energy is concentrated for $f < 2R_c$. In the present system, the RF bandwidth is pretty much set by the antenna frequency response at about 20 MHz. A good choice for the chip rate is therefore around 10 M chips/sec.

In the next figure, we see that the phase jitter reduces inversely with the notch filter bandwidth for a fixed chip rate. This phenomenon continues up to $f_N/R_c \approx 0.5$ (f_N is the 3 dB cutoff frequency for the notch filter) and the trend reverses itself as indicated in Fig. 11.3. In the first region, the notch filter suppresses the interference with a minimum distortion on the signal. After a critical point is reached the notch filter suppresses both the interference and the signal, and penalizes the latter more severely. The effect of the band center attenuation of the notch filter is shown in Figure 11.4. As to be expected, higher attenuation improves phase jitter performance. For $R_c = 10$ M chips/s, the phase noise contribution (suppressed) becomes negligible and the performance does not improve appreciably with increasing γ^2. In general, since the cost of the notch filter goes up with the attenuation, it seems logical to choose a value that is cost effective yet meeting the performance requirement.
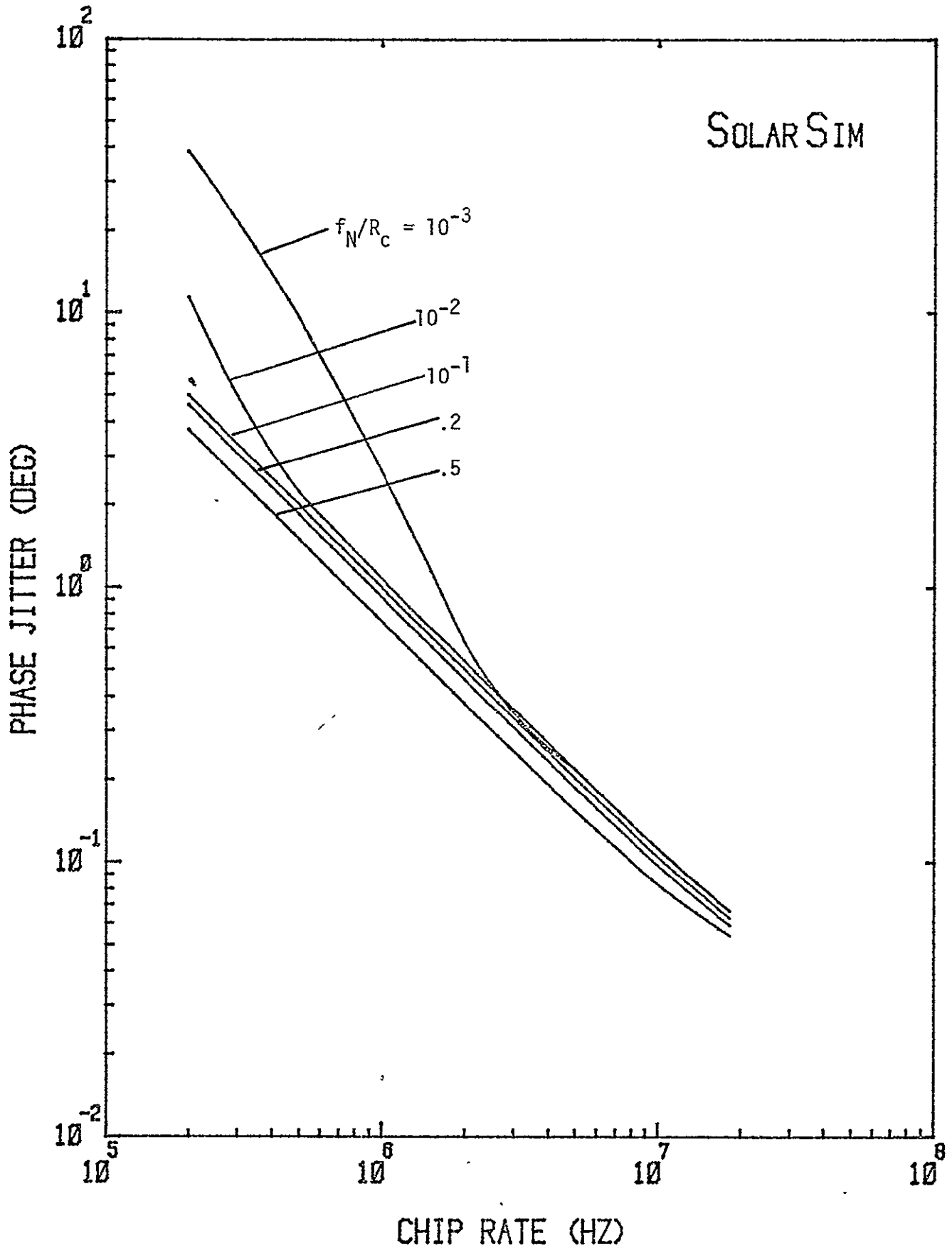
From Figure 11.5, we can observe that the phase jitter performance improves as the PN code period M is increased. As we have discussed earlier M is upper bounded by R_c/B_L. A reasonable choice is $M \approx 10^4$.

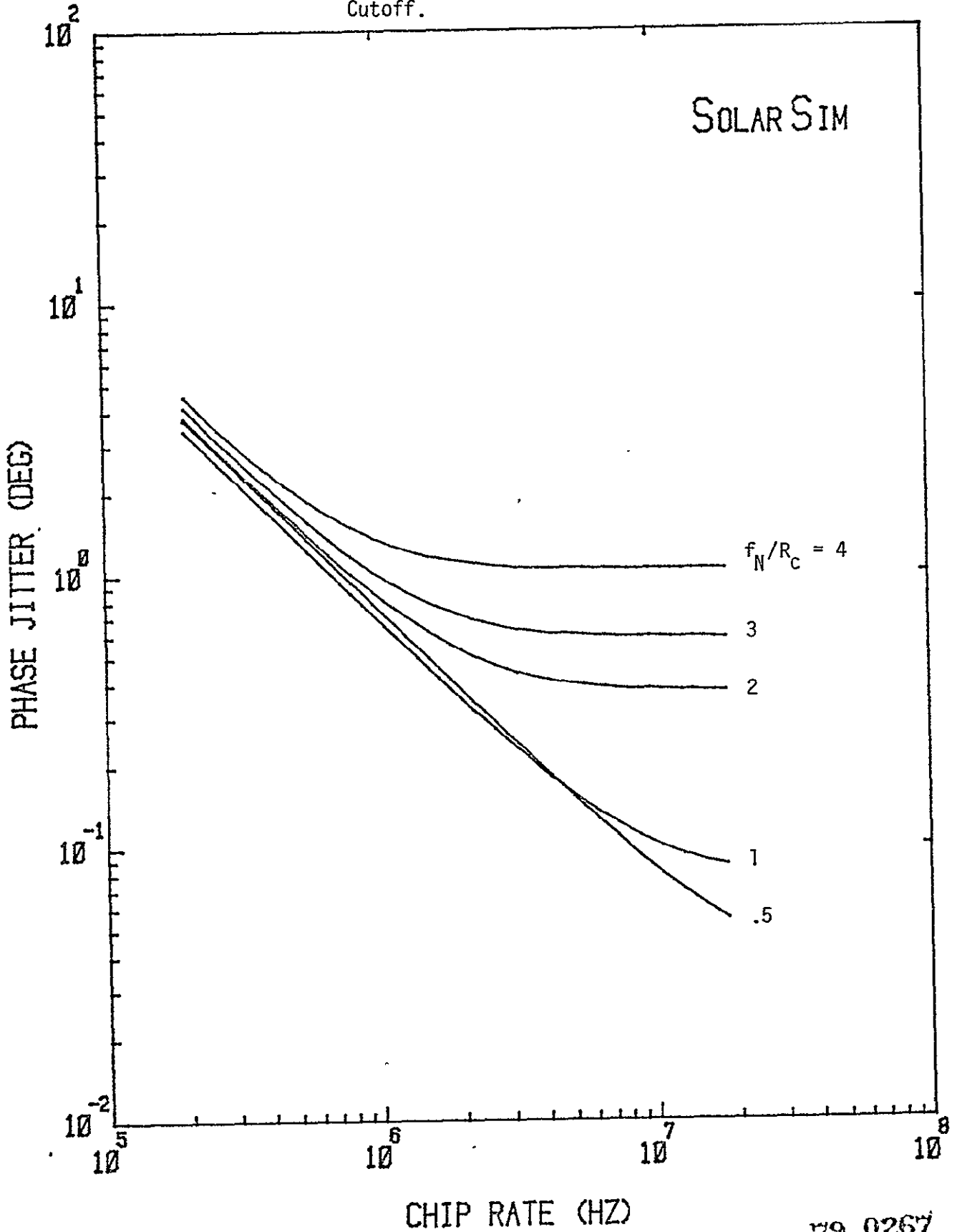Figure 11.1.   Effect of Varying RF Filter Cutoff Frequency.

SOLAR SIM

$f_{RF}/R_C = 0.5$

1

2

3

PHASE JITTER (DEG)

CHIP RATE (HZ)

'79 0265

Figure 11.2. Effect of Varying Notch Filter Frequency Cutoff.

SOLAR SIM

$f_N/R_C = 10^{-3}$

10^{-2}

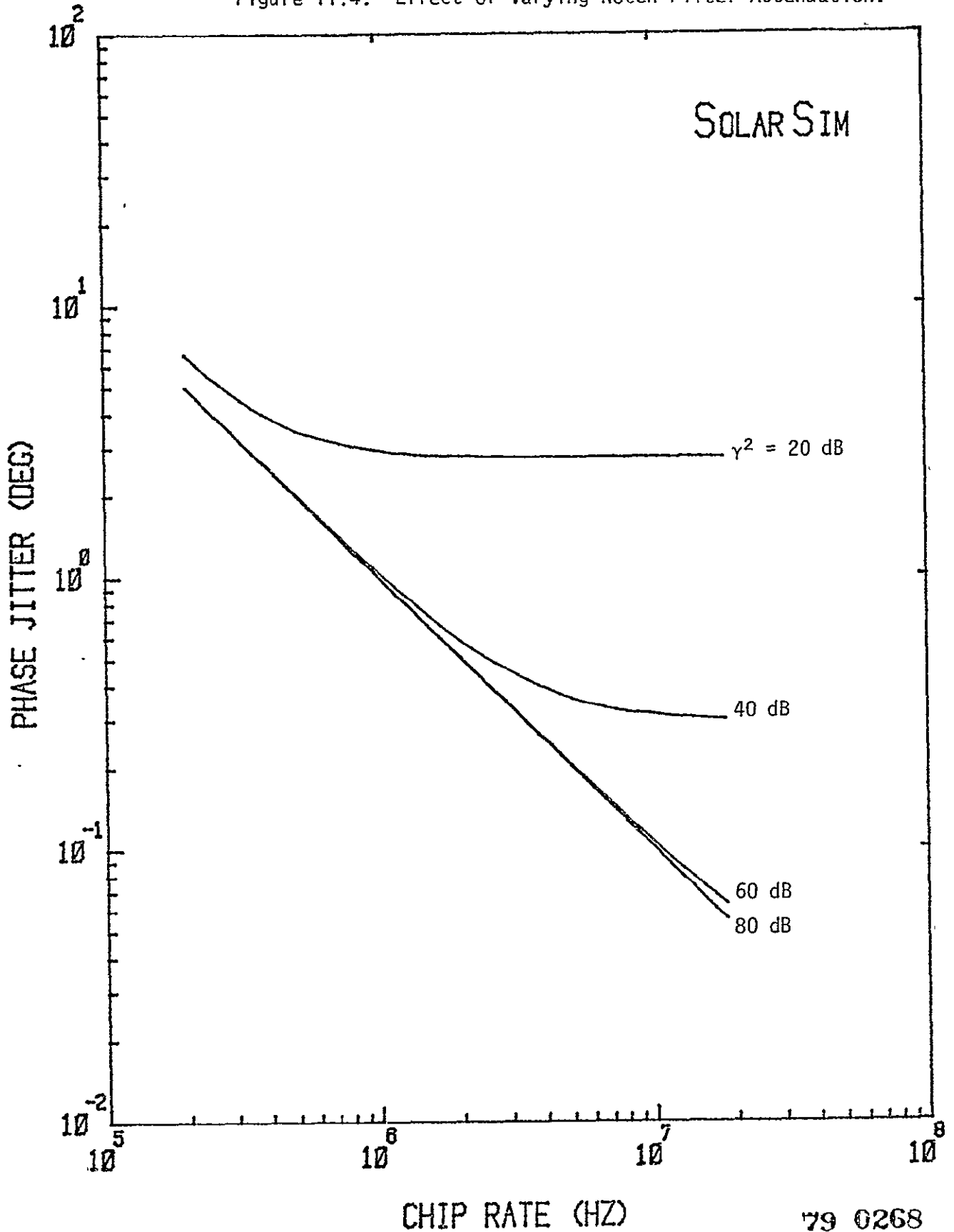10^{-1}

.2

.5

PHASE JITTER (DEG)

CHIP RATE (HZ)

79 0266

Figure 11.3. Effect of Varying Notch Filter Frequency
                    Cutoff.

Figure 11.4. Effect of Varying Notch Filter Attenuation.

Solar Sim

γ^2 = 20 dB

40 dB

60 dB
80 dB

PHASE JITTER (DEG)

CHIP RATE (HZ)

79 0268

Figure 11.5. Effect of Varying PN Code Period.

SOLAR SIM

M = 100

500

10^3

10^4

10^5

PHASE JITTER (DEG)

CHIP RATE (HZ)
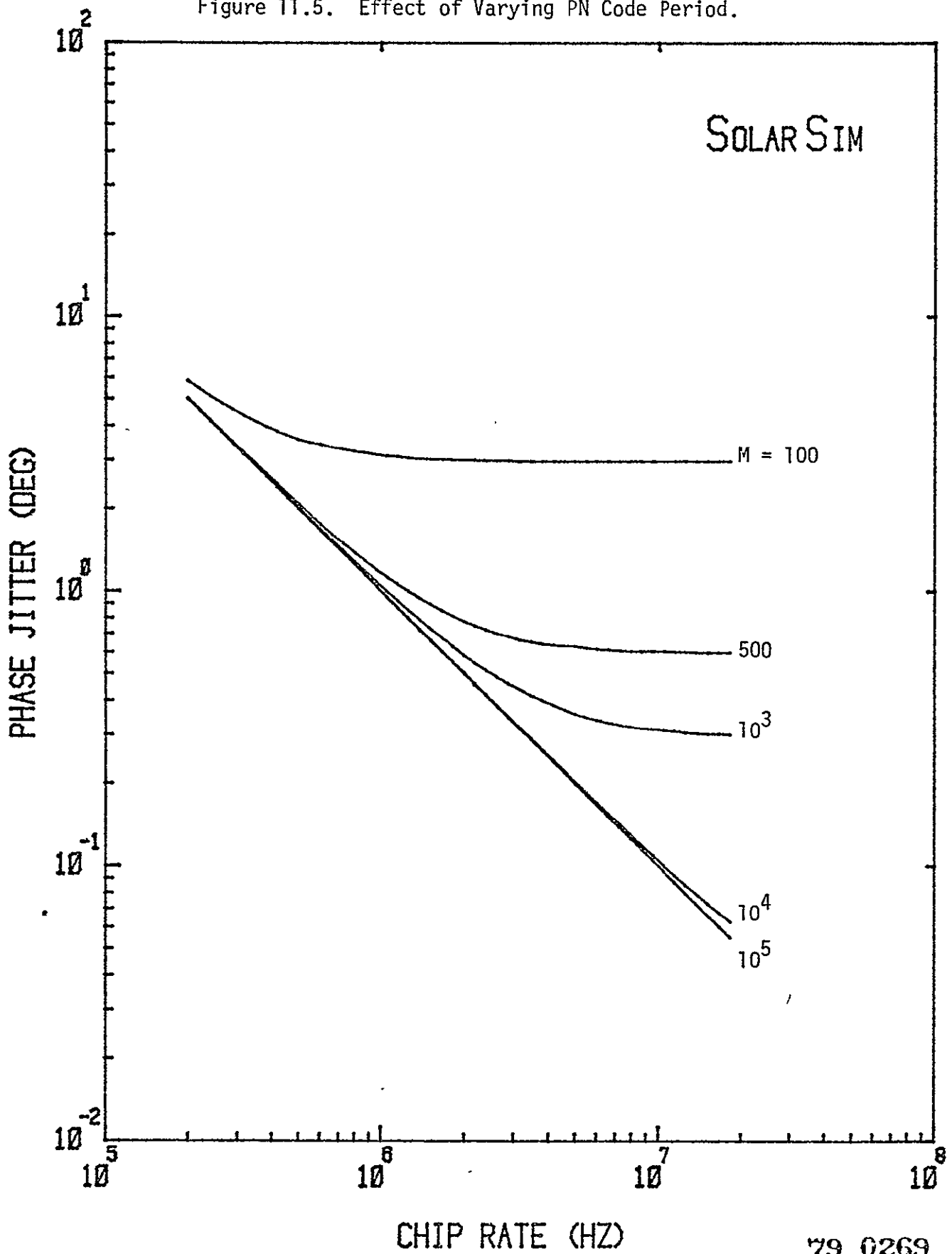
79 0269

12.0 REFERENCE SYSTEM SPS POWER TRANSPONDER

So far, we have considered the pilot receiver portion of the power transponder in conjunction with the selection of the uplink pilot signal parameters and the design of the transponder RF front end. In the following sections, we shall evaluate the overall system performance of the transponder. In particular, we shall proceed to characterize the transponder's ability to perform the phase conjugation in terms of the key technical issues specific to the SPS environment. Figure 12.1 represents the overall functional diagram of the SPS power transponder. This includes the pilot signal receiver, phase conjugation electronics and the high power amplifier phase control subsystem.

In the mechanization of the SPS power transponders, two receiver "types" will be required; however, most of the hardware will be common between two receivers. One receiver, the Pilot Spread Spectrum Receiver, is located at the center of the spacetenna or the reference subarray. It serves two major functions: (1) Acquires the SS code, the carrier and demodulates the command signal, (2) provides the main input signal to the Reference Phase Distribution System, see Figure 12.1.

The second receiver "type" will be located in the Beam Forming and Microwave Power Generating System, see Figure 12.2. Its main purpose is to phase conjugate the received pilot signal and trans-pond power via the j-th spacetenna element, $j = 1,2,...,101,552$. We now discuss the functional diagram indicating the mechanization of the SS power transponder and discuss its operation.

From Fig. 12.1 we note that each SS receiver element must be capable of despreading and demodulating the received pilot signal
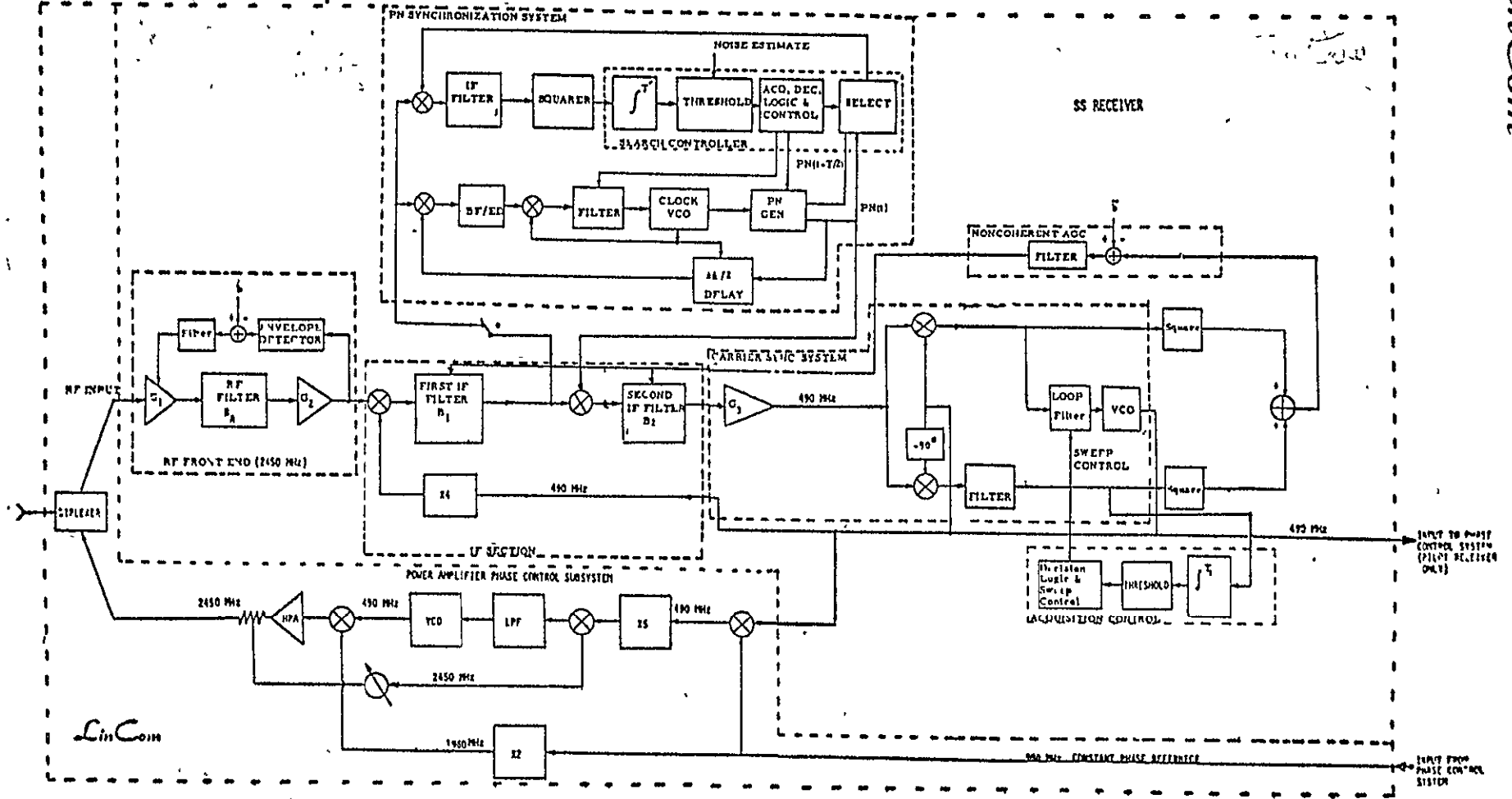
Figure 12.1. Central SPS Power Transponder Located at Spacetenna Center.
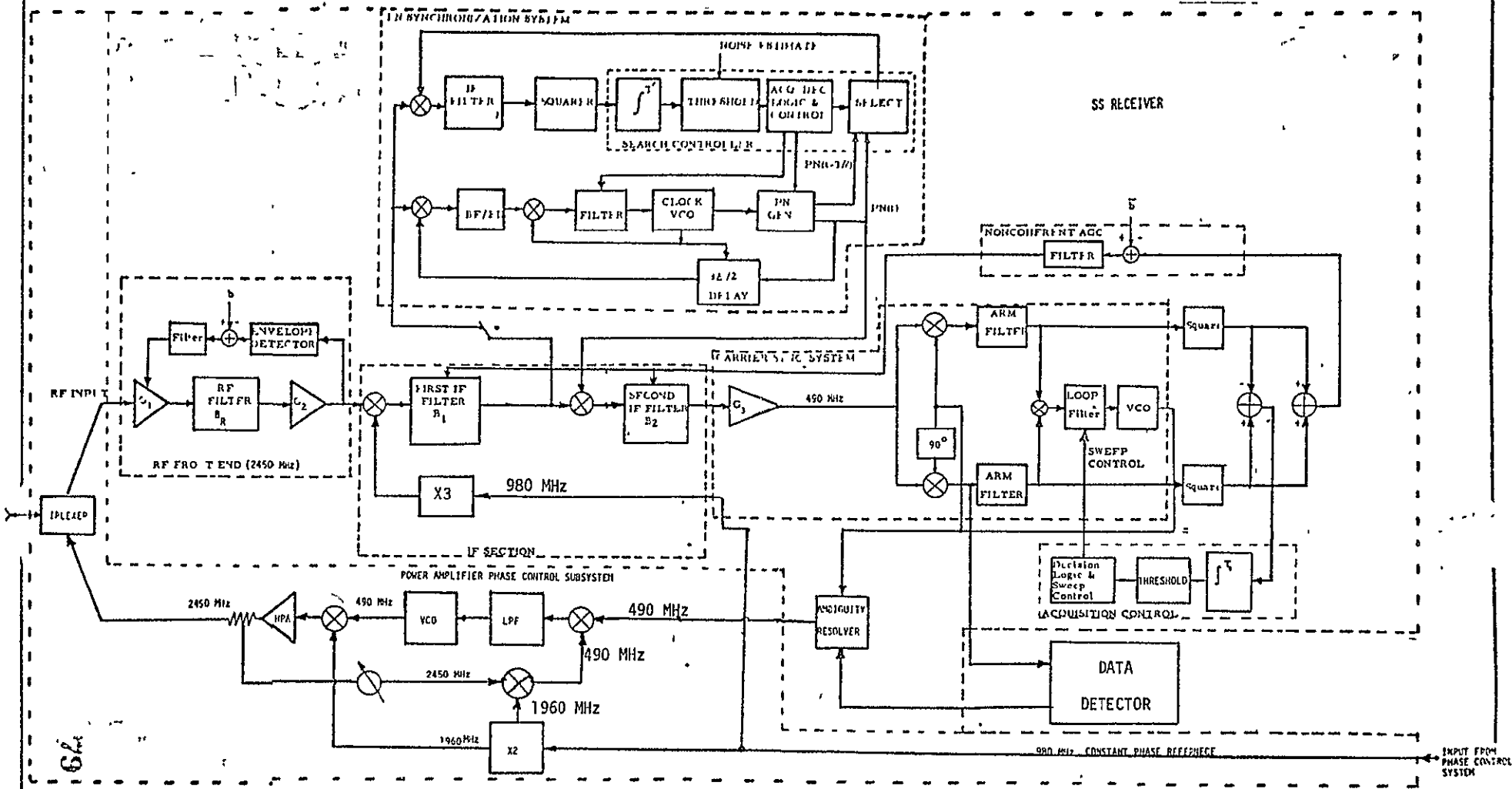
Figure 12.2. SPS Power Transponder

based upon the gain provided by a single element of the SPS space-
tenna. The receiver consists of several major subsystems. These
include, (see Figs. 5.1 and 5.2): (1) the RF Front End centered at
2450 MHz, (2) The SS Code (PN) Sync Subsystem (PNSS), (3) The AGC
Subsystems, (4) The Carrier Sync Subsystem (CSS), (5) The Carrier Lock
Detection Subsystem, (6) Carrier Sync Acquisition Subsystem, (7) Symbol
Synchronization Subsystem, (8) the Viterbi Decoder (if the uplink
employs convolutional coding), and (9) The Ambiguity Resolving Subsystem.
Note that (8) and (9) are not required if the pilot signal is not data
modulated.

The carrier, with nominal frequency of 2450 MHz, is first processed
via an RF filter. The bandwidth of this filter must be sufficiently
wide to pass the PN chips and the roll-off must be sufficient to meet
the desired rejection requirements.

The signal level into the first IF mixer is held constant by the
noncoherent AGC. The first LO is selected to run at 1960 MHz;
therefore, the first IF frequency, at zero Doppler, is 490 MHz. The
output of the first IF mixer is further filtered by the first IF filter
whose bandwidth is sufficiently wide to pass the PN chips. The cascaded
frequency response of the RF filter and the first IF filter are collect-
ively designed to meet the desired front end rejection requirements.
The IF filter output serves as the input to the PN synchronization
system. The PN sysnchronization system (PNSS) of Figure 12.1 incor-
porates a noncoherent τ-dither PN acquisition and tracking design.

The arriving NRZ/BPSK/BI-ϕ-DS/CDMA signal is despread prior to
filtering by the second IF filter. This gives rise to an ordinary
BPSK signal when the τ-dither loop is locked. The output from the

second IF filter goes to the output of the carrier recovery circuit. The bandwidth of the second IF filter is chosen to be wide with respect to the data rate.

A Costas (I/Q) loop configuration is chosen for carrier acquisition, tracking and data demodulation. This configuration was chosen because it was determined to be optimum when all considerations, including the ability to square perfectly over temperature and signal level, are traded against lock detection and synchronization monitoring.

Noncoherent AGC is derived from the sum "I" and "Q" Channels appearing in the arms of the Costas loop. In addition, lock detection for the carrier circuit is accomplished by using the difference between the "I" and "Q" channels of the Costas arms. The noncoherent AGC_2 controls the receiver gain (prior to phase detection) with the signal plus noise level appearing in the outputs of the Costas loop arm. This feature is used to control the loop bandwidth and damping factor during acquisition and tracking.

The loop filter receives the signals from the phase detector (third multiplier) and supplies an error signal to the VCO which control the local frequency. The loop filter sets the tracking loop bandwidth and damping factor. An AGC voltage, proportional to the incoming signal plus noise power, is low pass filtered and amplified to drive variable gain elements in the IF amplifiers. (These amplifiers are included here in the first and second IF filters for simplicity.) Additional integrate and dump circuits and threshold detector circuits control the sweep and the lock indicator needed for loop supervisory control. It is to be noted that the carrier sweep

is not activated until PNSS is synchronized.

The carrier lock detector circuit monitors the integrate and dump voltage formed at the discrete points in time by differencing the squares of the inphase and quadrature arm outputs. The output of the integrate and dump circuit is compared to a fixed threshold level to detect lock.

If the pilot signal is data modulated, the data can be extracted from the output of the Q-channel as shown in Fig. 12.2. The 180 degree phase ambiguity the Costas loop introduced can be resolved by periodically inserting a (predetermined) identification sequence in the transmitted data stream; the recovered data can be checked against this known pattern to correct for the phase ambiguity. When the pilot signal is not data modulated, the Costas loop can be replaced by a CW loop. This avoids the need for provisions in the carrier tracking subsystem to resolve phase ambiguity.

The 490 MHz reference appearing at the pilot receiver VCO output, see Figure 12.1, serves as the only input to the Phase Control System. This phase characteristic is then distributed over the aperture of the spacetenna. The output of the Phase Control System consists of 101,552 980 MHz constant phase reference signals which are used to conjugate the incoming signal and to stabilize the high power amplifier (HPA) outputs. This is achieved by placement of an automatic phase control around each HPA, see Figure 12.2.

13.0 SIGNAL AND NOISE CHARACTERISTICS

For the purpose of the SPS transponder analysis, the signal and noise spectrum into the transponder can be represented as shown in Fig. 13.1. The spectral shape of the input Bi-ϕ-PN spread pilot signal

COHERENT PHASE NOISE
INTERFERENCE, K_2

NONCOHERENT PHASE NOISE
INTERFERENCE, K_1

f_N ——NOTCH FILTER

f_{RF}

←RF FILTER

RECEIVER NOISE
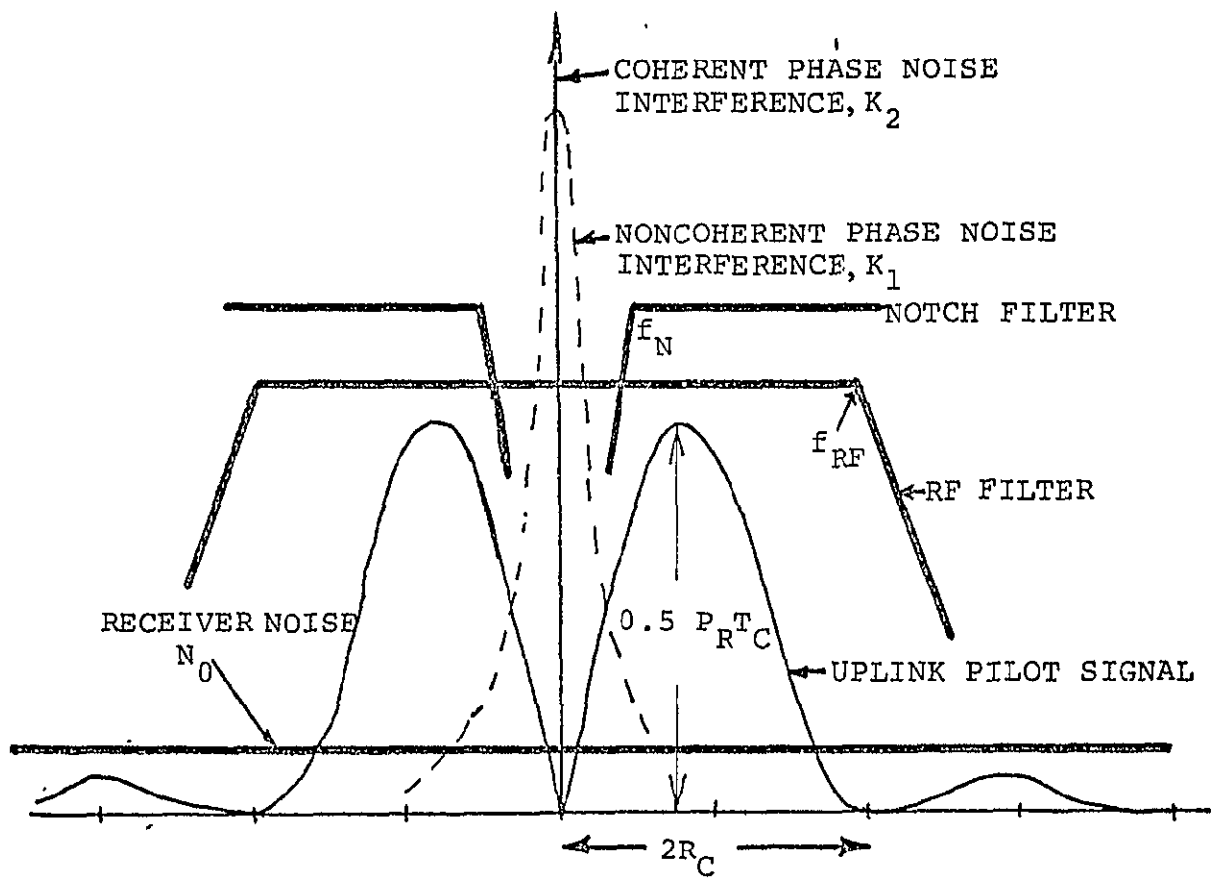N_0

$0.5\ P_R T_C$

←UPLINK PILOT SIGNAL

$2R_C$

Figure 13.1. Signal and Noise Spectrum into SPS Transponder.

is of the form $\sin^4(x)/x^2$ with the nulls occurring at frequency multiples of $2R_c$ (R_c = PN chip rate). The receiver front end contributes an equivalent thermal noise level equal to N_0 W/Hz. The phase noise interferences from the power beams (including its own) can be modeled by the coherent and noncoherent terms and indicated. The important RF filter and notch filter characteristics are also shown in the same figure. The RF filter is used to model the bandwidth of the receiving antenna (waveguide arrays). The notch filter is introduced to suppress the phase noise interferences. It is clear that since the portion of the signal power close to the carrier is small, the signal distortion introduced by the notch filter is negligible while the interferences can be significantly suppressed. The optimal selection of the filter parameters have been considered in the preceding sections.

The klystron amplifier in the power transponder generates a phase noise profile that can add significantly to the downlink carrier phase error if it is unattended for. Figure 13.2 shows the phase noise sideband power spectral density measured on a Varian X-13 klystron amplifier,* which we have adopted as our klystron model. Upon reflecting to 2.45 GHz, the phase noise component that is outside a bandwidth B_L is plotted in Fig. 13.3. Selected values are tabulated in Table 13-1. The components of the klystron phase noise around the carrier frequency can be tracked with the PA phase control loop provided for in the reference system. With the loop around the klystron, only phase noise components which have Fourier frequencies greater than

---

*The complimentary measurement is provided to LinCom by Dr. Algie Lance of TRW, Redondo Beach, CA.
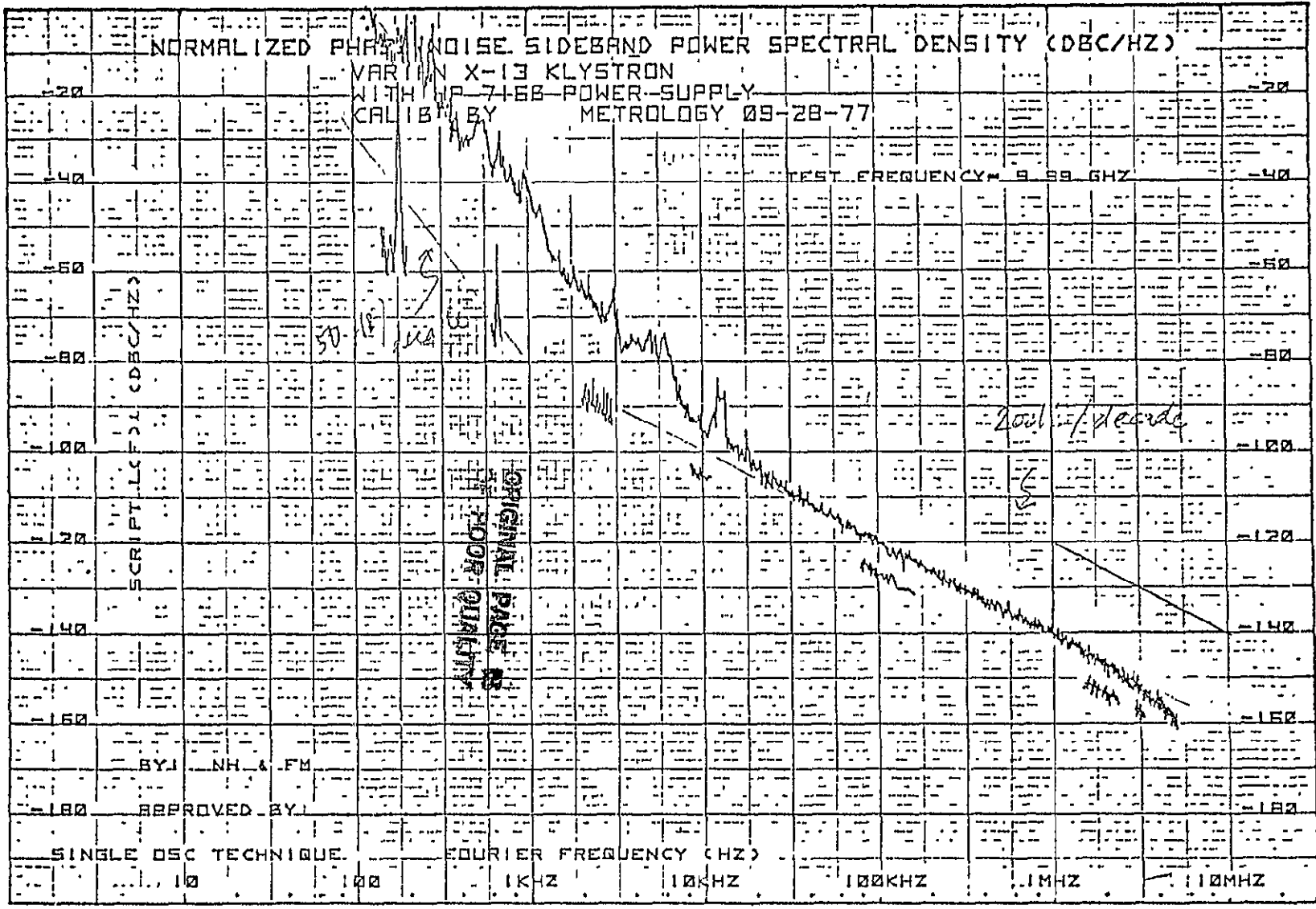
Figure 13.2. Normalized Phase Noise Sideband Power Spectral Density of a Varian X-13 klystron Tube (courtesy of Dr. Algie Lance, TRW).
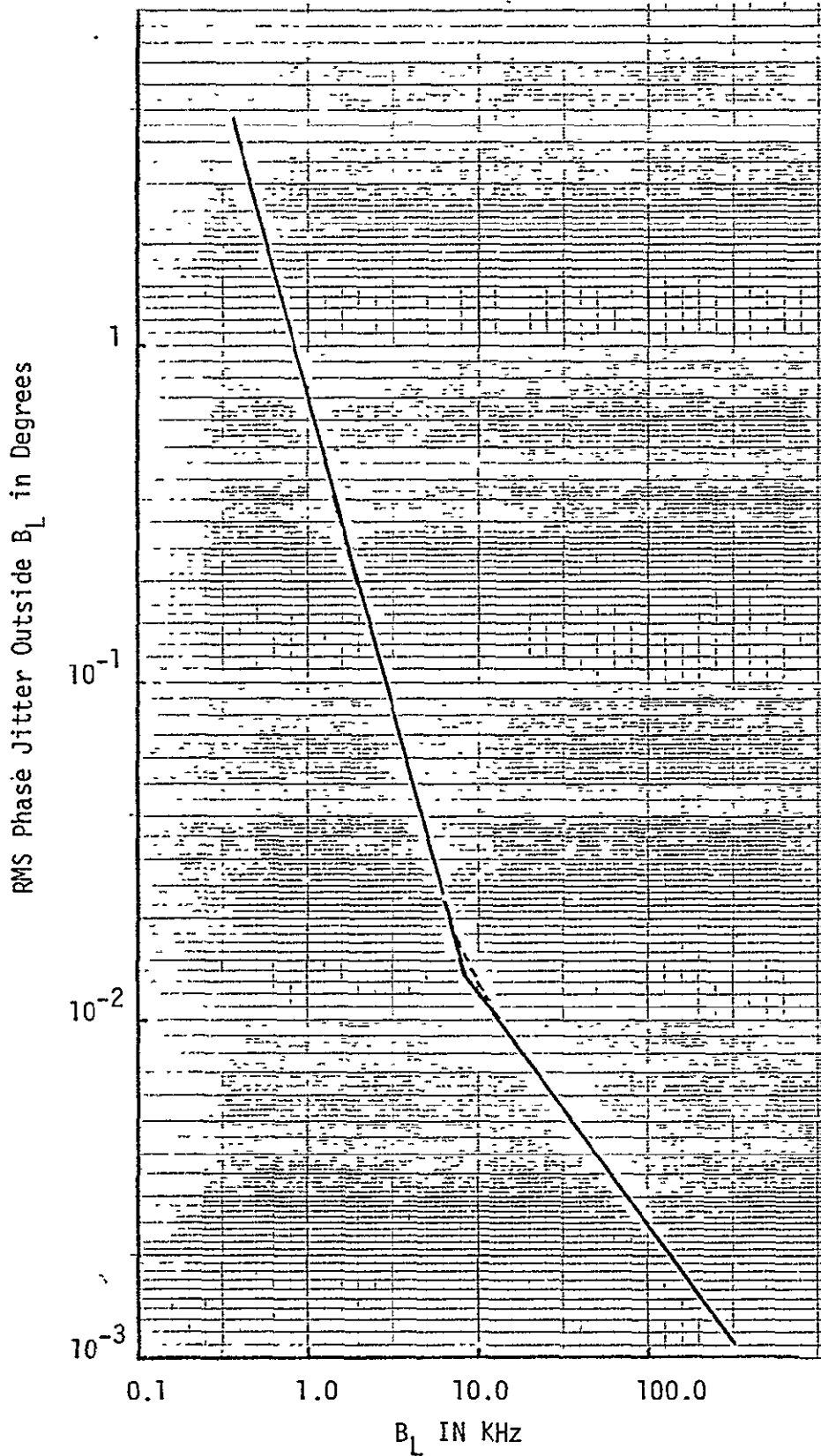
Figure 13.3. A Plot of rms Klystron Phase Noise Outside a Bandwidth B_L.

Table 13-1. Phase Noise Component Outside an Ideal Tracking
Loop with Bandwidth B_L.

BANDWIDTH, B_L (Hz)	RMS PHASE NOISE (deg)	
	AT 10 GHz	AT 2.5 GHz
100 KHz	10^{-2}	2.5×10^{-3}
10 KHz	5×10^{-2}	1.25×10^{-2}
1 KHz	3	0.75
400 Hz	20	4

B_L will be transmitted. Components below this frequency will be suppressed by a factor 1-H(s) where H(s) is the closed-loop transfer function of the PA control loop. Assuming an ideal loop transfer function, namely H(f) = 1 for f < B_L and H(f) = 0 for f $\geq$ B_L, we can predict the amount of phase noise leakage through the transmitter. For example, from Table 13-1 a 400 Hz loop will introduce a rms phase error of 4 degrees. When the phase noise effect is the only consideration, the obvious solution is to widen the loop bandwidth as far as possible. However, this also opens up the bandwidth for other noise contributions through the transponder. Clearly, a tradeoff has to be made to yield an optimum balance. A more detailed modeling of the overall system which enables such a tradeoff will be addressed in Section 14.0.

Other noise sources that affect the performance of the transponder includes the VCXOs, mixers, multipliers, up converters and down-converters. Their relevance will also be discussed in Section 14.0.

14.0 <u>SPS TRANSPONDER TRACKING LOOP SUBSYSTEMS</u>

At the proposed synchronous orbit, the channel Doppler profile is characterized by a maximum Doppler of 25 Hz and a maximum Doppler rate of 2×10^{-3} Hz/sec, at the carrier frequency of 2,450 MHz. For this reason, loop acquisition does not pose any significant problem. The loop bandwidths can be made to be relatively small (as low as two Hz) and still guarantees satisfactory response time.

14.1 <u>PN Tracking Loop</u>

The main purpose of the PN tracking loop is to despread the incoming Bi-ϕ-PN signal. It is not designed for Doppler or range measurement. As such, the tracking error requirement is not very critical as long as it is limited to a few percent of a chip time.

PN acquisition will take time from a "cold start," i.e., when the local PN clock is not running. This can occur, for example, when the system is powered on initially. In that case, the local clock has to step over all possible code states during acquisition. However, once the local clock starts running, it should be almost synchronous with the ground code due to the almost nonexistent channel Doppler. If the local clock is left running when the system is brought down for whatever reasons, the latter can be brought back up using the local clock. No additional acquisition algorithm is required.

Since all power transponders are experiencing the same Doppler for all practical purposes, a way to cut down the acquisition time and individual acquisition hardware requirement is to include a separate telemetry receiver that tracks the uplink pilot. This pilot signal is constantly tracked by the telemetry receiver and the state of the local PN clock can be transferred to the individual transponders to start the PN loops. In that case, no acquisition aid on the transponders are required. However, data links between the telemetry receiver and the transponders must be established.

In the reference system, a τ-dither loop is used to avoid the gain imbalance problem commonly found in the standard delay-lock loop implementation. Fig. 14.1 gives an alternate implementation [8] of the delay-lock loop which is immune to gain imbalances and is equivalent to the classical delay-lock loop. The delay-lock loop can potentially outperform the τ-dither loop by approximately 1 dB.

14.2 Phase Reference Tracking Loop Model

Fig. 14.2 shows the equivalent mathematical model of the phase reference tracking loop located at the center of the spacetenna.
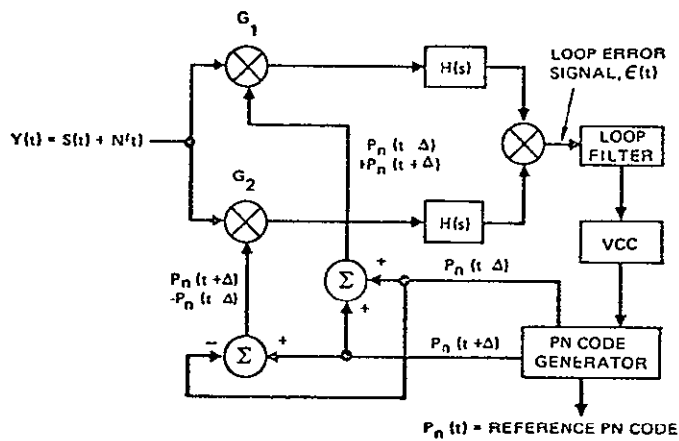
Figure 14.1. A Delay-Lock Loop Implementation Insensitive
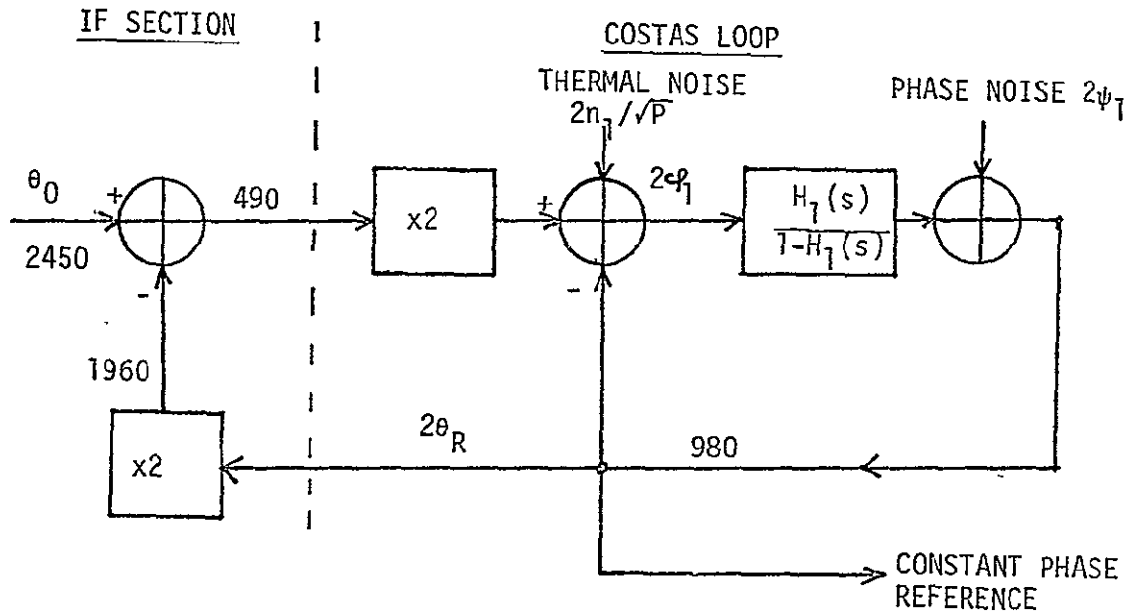to Arm Gain Imbalance.

'79 0275

Figure 14.2. 980 MHz Constant Phase Reference Tracking
Loop Model.

79 0281

The phase reference tracking loop is mechanized as a long loop. The statistics of the loop phase error φ_1 and the phase of the reference θ_R (both measured at 490 MHz) are of importance to assess performance. In the tracking mode, they are related to the input noise processes via

$$\varphi_1 = \frac{1-H_1(s)}{1+4H_1(s)}(\theta_0 - 5\psi_1) - \frac{H_1(s)}{1+4H_1(s)}\left(\frac{5n_1}{\sqrt{P}}\right) \tag{14-1}$$

$$\theta_R = \frac{1-H_1(s)}{1+4H_1(s)}\psi_1 + \frac{H_1(s)}{1+4H_1(s)}\left(\frac{n_1}{\sqrt{P}} + \theta_0\right) \tag{14-2}$$

where θ_0 is the transmit phase noise including the ionospheric disturbances, n_1 is the equivalent thermal noise seen by the loop, P is the transmitted power seen by the loop, ψ_1 models the equivalent VCO/mixer phase noise and $H_1(s)$ represents the closed loop transfer function of the Costas loop. The squaring loop mechanization also introduces a squaring loss which is a function of the arm filters and the IF filter bandwidth preceding the I-Q phase detectors. This factor must be accounted for, presumably in computing n_1 before using (14-1) and (14-2) for performance evaluations.
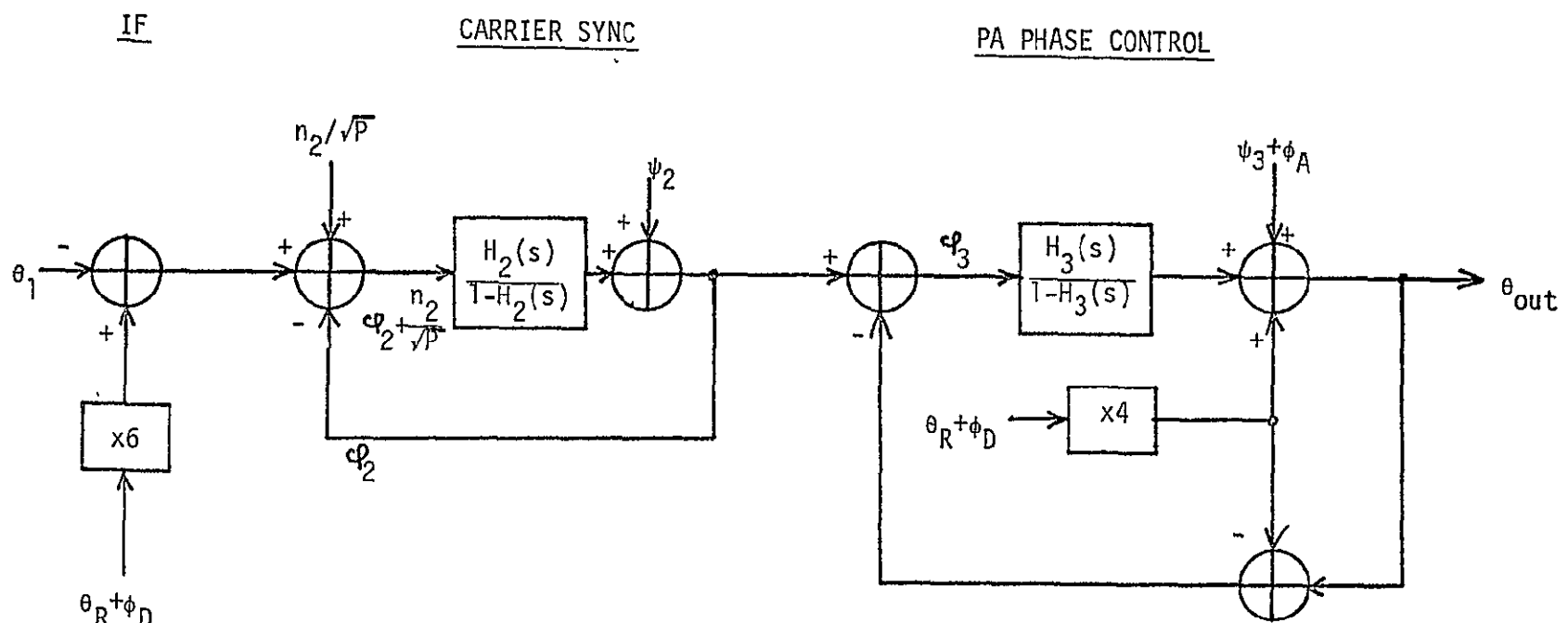
14.3 Power Transponder Phasing System Model

The equivalent mathematical model of the individual transponders is given in Fig. 14.3. The relevant tracking equations for the pilot phase recovery loop are

$$\varphi_2 = [1-H_2(s)][6(\theta_R+\phi_D)-\theta_1] - [1-H_2(s)]\psi_2 - H_2(s)\frac{n_2}{\sqrt{P}} \tag{14-3}$$

and

$$\theta_2 = [1-H_2(s)]\psi_2 + H_2(s)\left[\frac{n_2}{\sqrt{P}} + 6(\theta_R+\phi_D) - \theta_1\right] \tag{14-4}$$

where φ_2 is the tracking error, θ_1 the transmit pilot phase noise, ψ_2 models the equivalent VCO/mixer phase noise, n_2 is the equivalent thermal

IF

CARRIER SYNC

PA PHASE CONTROL

$n_2/\sqrt{P}$

ψ_2

$\psi_3+\phi_A$

θ_1

$+$

$-$

$+$

$\dfrac{H_2(s)}{1-H_2(s)}$

$\dfrac{n_2}{\sqrt{P}}$

$\psi_2+\dfrac{n_2}{\sqrt{P}}$

ψ_2

φ_3

$\dfrac{H_3(s)}{1-H_3(s)}$

θ_{out}

x6

$\theta_R+\phi_D$

$\theta_R+\phi_D$

x4

θ_R: 490

θ_1:   2450

Figure 14.3.   Power Transponder System Model.

noise, P the transmitted pilot power, $H_2(s)$ is the closed loop transfer function for the Costas loop and ϕ_D models the phase noise and differential delay introduced by the phase distribution system. The relevant tracking equations for the PA phase control loop are

$$\varphi_3 = [1-H_3(s)]\theta_2 - [1-H_3(s)](\phi_A+\psi_3) \qquad (14\text{-}5)$$

$$\theta_{out} = [1-H_3(s)](\phi_A+\psi_3) + H_3(s)\theta_2 + 4(\theta_k+\phi_D) \qquad (14\text{-}6)$$

where φ_3 is the loop phase error, $H_3(s)$ is the closed loop transfer function, ϕ_A is the (PA) klystron phase noise, and ψ_3 models the VCO/ mixer phase noise. The noise process θ_{out} is the single most important quantity as it models the phase error process at the output of the transponder and it directly affects the efficiency performance of the SPS. Note that except for the klystron phase noise which is measured at 2450 MHz, all other phase noise processes are measured at 490 MHz.

14.4 Overall Transponder Equivalent System Model for Analysis

The analytical model for the performance of the overall transponder is given in Fig. 14.4. Notice that the inputs to the transponders are θ_0, θ_1, n_1 and n_2; θ_0 and θ_1 represent the phase noise on the pilot signal including the effects of the ionospheric disturbances and transmit frequency instability and n_1 and n_2 represents the effects of the receiver thermal noise, power beam interferences ('caused by mutual coupling) and data distortions. The phase disturbance at the output of the transponder is the term of interest as it directly affects power transfer efficiency of the SPS. We have studied this effect extensively using the SOLARSIM program. All other noise components are generated within the power transponder. They are the filtered version of various hardware induced noises.
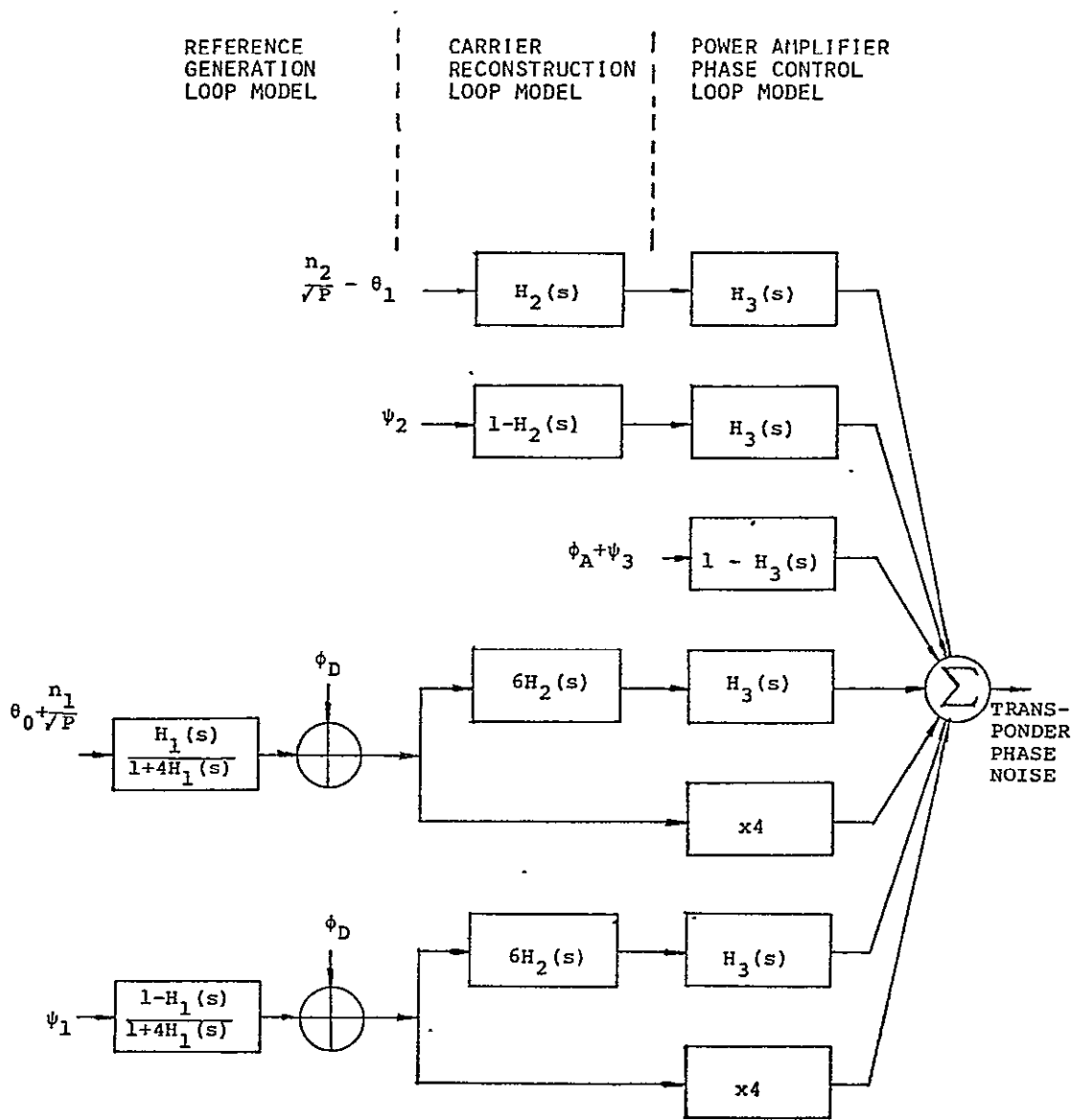
Figure 14.4. Overall Transponder Equivalent System Model for Analysis.

In Fig. 14.4, filters of the form H(s) are low pass filters and filters of the form 1-H(s) are high pass filters. Note that oscillator phase noises (including the klystrons) are all filtered by a high pass filter. Since oscillator phae noise profiles are typically of the form indicated in Fig. 14.5 with most of the phase noise power concentrated around the carrier, one should widen H(s) as far as possible. For example with our klystron model, the bandwidth of $H_3(s)$ should be kept to approximately 1 KHz to limit the phase noise introduced jitter to less than 1 degree. However, widening H(s) also introduces other problems. As another example, opening up $H_2(s)$ and $H_3(s)$ allows more phase jitter due to n_2 and θ_1. Obviously, in order to attain the optimum choice of loop bandwidths, we need to specify power spectral densities of all the noise processes, and then perform tradeoffs based on the system model. In view of the fact that many parameters are involved, a simulation program is needed to exercise these tradeoffs.

A careful examination of Fig. 14.4 also reveals the following important fact: some of the noise processes are irreducible. For example, one can reduce the effects of $n_2/\sqrt{P}$ by changing the system designs such as reducing the bandwidths of $H_2(s)$ and $H_3(s)$, increasing the uplink power, · increasing the processing gain of the PN signal or employing diplexers with improved isolation characteristic, etc. However, there is nothing one can do about the random phase disturbance ϕ_D introduced by the phase distribution tree because a major portion of ϕ_D appears at the transponder output unmodified. From Fig. 14.4, one can see that the irreducible error terms are ϕ_D and the ionospheric differential phase perturbations θ_0 and θ_1. (The processes θ_0 and θ_1 can have a significant portion of power within typical values of loop bandwidths.)
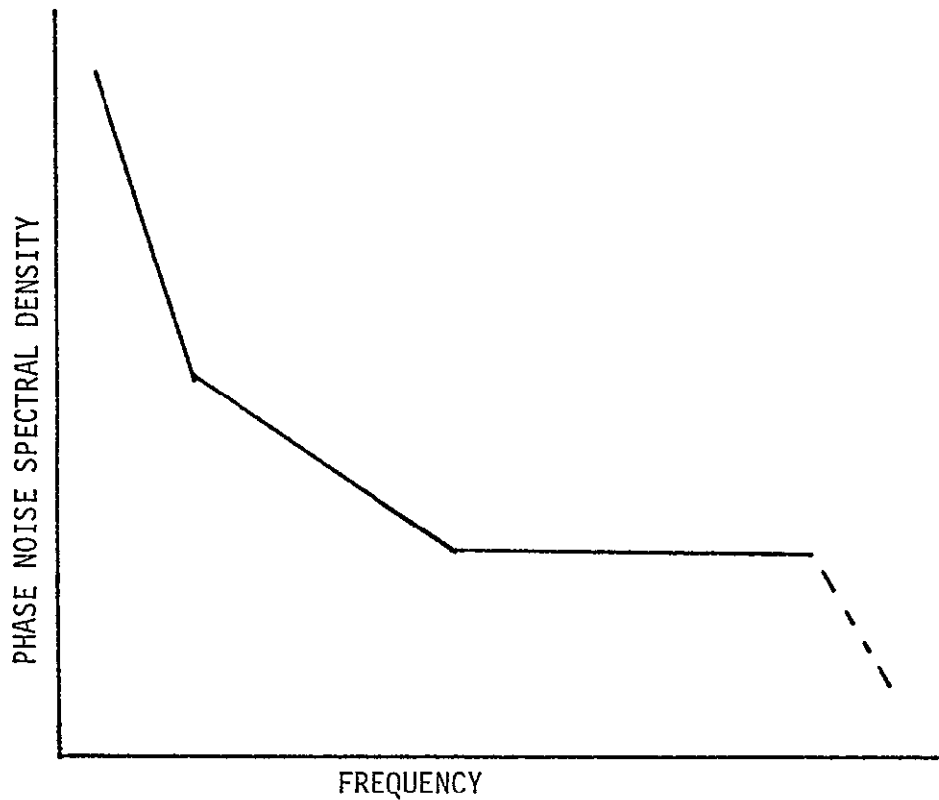
Figure 14.5.   Typical Oscillator Phase Noise Profiles.

15.0 RECOMMENDATION FOR OVERALL TRANSPONDER DESIGN

Although a thorough simulation study is required to quantify various tradeoffs, one can still make some general recommendations on the transponder design. From the power transfer efficiency study, we know that the transponder phasing system have to hold its rms phase error to under 10 degrees. In that case, it is reasonable to limit the contributions from each individual error source to less than 1 degree rms. Under this guideline, we can make the following recommendations:

(1) Klystron phase control loop bandwidth $\geq$ 10 KHz.

(2) Code loop jitter can be made negligible and is not critical to performance.

(3) Costas loop bandwidth $\approx$ 10 Hz.

When these conditions are met, it is reasonable to expect that the rms phase error introduced by the transponder, interference and thermal can be limited to less than one degree. However, this does not take into account the effects of the reference phase distribution error and the hardware induced differential delay variations that differs from transponder to transponder. Unfortunately, these effects belong to the class of irreducible errors that cannot be controlled by the transponder design.

LinCom

References

[1] W. C. Lindsey, "A Solar Power Satellite Transmission System Incorporating Automatic Beam Forming, Steering and Phase Control," LinCom Report TR-7806-0977, June 1978.

[2] R. A. Scholtz, "The Spread Spectrum Concept," IEEE Trans. on Comm., Vol. COM-25, No. 8, August, 1977, pp. 748-755.

[3] W. Peterson and E. Weldon, Error Correcting Codes, Wiley, 1972.

[4] R. Gold, "Optimum Binary Sequences for Spread Spectrum Multiplexing," IEEE Transactions on Information Theory, Oct. 1967.

[5] H. F. A. Roefs, Binary Sequences for Spread Spectrum Multiple Access Communication, Coordinated Science Laboratory Report R-875, University of Illinois, Aug. 1977.

[6] J. D. Olsen, R. A. Scholtz, and L. R. Welch, "Bent Function Sequences," submitted to IEEE Transactions on Information Theory.

[7] W. C.Lindsey and M. K. Simon, Telecommunication Systems Engineering, Prentice-Hall, 1973.

[8] D. T. LaFlame, "A Delay-Lock Loop Implementation Which is Insensitive to Arm Gain Imbalance," IEEE Trans. Comm. Tech., COM-27, Oct. 1979, pp. 1632-1633.

LinCom

APPENDIX 1

BASEBAND-EQUIVALENT FILTERING

Let

$$x(t) = \mathrm{Re}\left\{m(t)e^{j\omega_c t}\right\}$$

$$= \frac{1}{2}m(t)e^{j\omega_c t} + \frac{1}{2}m^*(t)e^{-j\omega_c t}$$

Taking Fourier transforms,

$$X(f) = \frac{1}{2}M(f-f_c) + \frac{1}{2}M^*(-f-f_c)$$

Suppose we pass this through a filter with real impulse response $H(f) = H^*(-f)$. Then the output $y(t)$ has transform
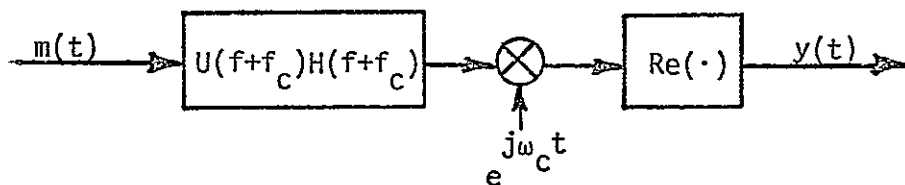
$$Y(f) = H(f)[\frac{1}{2}M(f-f_c) + \frac{1}{2}M(-f-f_c)]$$

Now if $|M(f)| = 0$ for $|f| \geq f_c$, then

$$Y(f) = \frac{1}{2}U(f)H(f)M(f-f_c) + \frac{1}{2}U(-f)H^*(-f)M^*(-f-f_c)$$

Hence since $Y(f)$ has conjugate symmetry

$$y(t) = \mathrm{Re}\left\{\int_0^\infty H(f)M(f-f_c)e^{j\omega t}df\right\}$$

$$= \mathrm{Re}\left\{e^{j\omega_c t}\int_{-\infty}^\infty U(f+f_c)H(f+f_c)M(f)e^{j\omega t}df\right\}$$

$y(t)$ can now be modelled as follows:

BASEBAND-EQUIVALENT MULTIPLICATION

Let

$$x(t) = \text{Re}\{a(t)e^{j\omega_1 t}\}$$

$$y(t) = \text{Re}\{b(t)e^{j\omega_2 t}\}$$
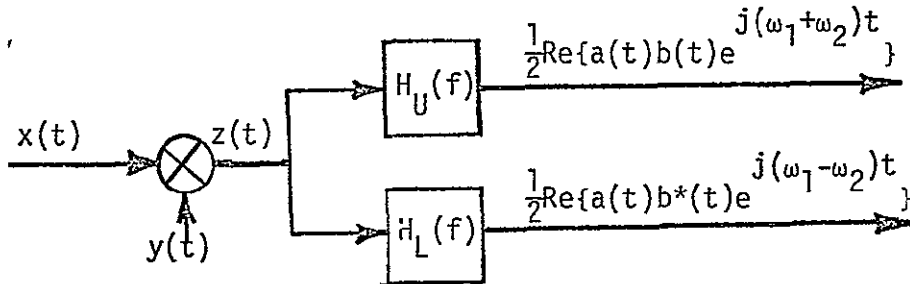
and suppose that

$$z(t) = x(t)y(t).$$

Then

$$z(t) = \frac{1}{2}\text{Re}\{a(t)b(t)e^{j(\omega_1 + \omega_2)t} + a(t)b^*(t)e^{j(\omega_1 - \omega_2)t}\}$$

Now suppose that $a(t)$ and $b(t)$ are bandlimited so that

$$A(f) = 0, \quad |f| > B_A$$

$$B(f) = 0, \quad |f| > B_B$$

Then the two components of $z(t)$ can be recovered by filtering

when

$$f_1 > f_2 > B_A + B_B > 0$$

$$H_U(f) \approx \begin{cases} 1, & ||f| - (f_1 + f_2)| < B_A + B_B \\ 0, & ||f| - (f_1 - f_2)| < B_A + B_B \end{cases}$$

$$H_L(f) \approx \begin{cases} 1, & ||f| - (f_1 - f_2)| < B_A + B_B \\ 0, & ||f| - (f_1 + f_2)| < B_A + B_B \end{cases}$$

APPENDIX 3

THE PRODUCT FILTERING APPROXIMATION

Suppose that

$$z(t) = x(t)y(t)$$

and that $z(t)$ is the input to a linear filter whose output is $w(t)$,

$$w(t) = \int_{-\infty}^{\infty} x(\alpha)y(\alpha)h(t-\alpha)d\alpha$$

Now suppose that $x(t)$ is reasonably constant over the periods corresponding to the duration of the impulse response $h(t)$. It is then possible to approximate $w(t)$ by

$$w(t) \approx x(t) \int_{-\infty}^{\infty} y(\alpha)h(t-\alpha)d\alpha$$

This assumes $h(t)$ is nonzero primarily near $t=0$.

APPENDIX 4

SS CODE SPECTRAL DENSITY

The SS code signal $c_R(u,t)$ is periodic with period MT_c where M is the period of the sequence $\{a_i\}$. The correlation function can be found simply by time averaging the correlation product over one period

$$R_{c_R}(\tau) = \frac{1}{MT_c} \int_{-T_c/2}^{MT_c-T_c/2} c_R(u,t+\tau)c_R(u,t)dt$$

with $\hat{\tau}(u)$ set to zero

$$R_{c_R}(\tau) = \frac{1}{MT_c} \sum_{i=0}^{M-1} \sum_{j} a_i a_j \int_{-T_c/2}^{MT_c-T_c/2} P(t-iT_c)P(t-jT_c-\tau)dt$$

Setting $\tau = mT_c+\tau_0$, $0 \leq \tau_0 < T_c$, we can use the fact that $P(t)=0$ for all $|t| < T_c/2$ to simplify this to

$$R_{c_R}(\tau) = R_a(m)R_p(\tau_0) + R_a(m+1)R_p(\tau_0-T_c)$$

where

$$R_a(m) = \frac{1}{M} \sum_{i=0}^{M-1} a_i a_{i+m}$$

$$R_p(\tau_0) = \frac{1}{T_c} \int_{-T_c/2}^{T_c/2} P(t)P(t-\tau_0)dt$$

It is apparent that $R_{c_R}(\tau)$ is periodic with period MT_c and hence has a line power spectral density

$$S_{c_R}(f) = \sum_{n} P_n \delta\left(f - \frac{n}{MT_c}\right)$$

where $\delta(f)$ is the Dirac delta function and P_n is given by

$$P_n = \frac{1}{MT_c} \int_0^{MT_c} R_{c_R}(\tau) e^{-j2\pi n\tau/MT_c} d\tau$$

$$= S_a(n) \left| \frac{p(f)}{T_c} \right|^2_{f=n/MT_c}$$

where $p(f)$ is the Fourier transform of $P(t)$ and $S_a(n)$ is the discrete Fourier transform of $R_a(m)$:

$$S_a(n) = \frac{1}{M} \sum_{m=0}^{M-1} R_a(m) e^{-j2\pi nm/M}$$

For the standard Bi-ϕ Manchester waveform

$$p(f) = \int_{-\infty}^{\infty} P(t) e^{-j2\pi ft} dt$$

$$= \frac{2}{-j\pi f} \sin^2(\pi f T_c/2)$$

whence

$$P_n = S_a(n) \frac{4 \sin^4(\pi f T_c/2)}{\pi^2 f^2}$$

APPENDIX 5

THE SPECTRAL DENSITY OF $A_k(u,t)$

The quantity $A_k(u,t)$ is a complex-valued multiplicative noise factor appearing in the downlink transmitter modulation for subarray k. It is assumed independent of $A_j(u,t)$, $j \neq k$. We shall suppress the subscript k and expand $A_k(u,t)$ in an envelope and phase representation:

$$A(u,t) = |A(u,t)|e^{j\theta(u,t)}$$

Lets further assume that $\theta(u,t)$ is Gaussian and independent of $|A(u,t)|$ so that the autocorrelation function of $A(u,t)$ is given by

$$R_A(\tau) = R_{|A|}(\tau)R_{ph}(\tau)$$

where

$$R_{ph}(\tau) = E\{\exp(j[\theta(u,t+\tau)-\theta(u,t)])\}$$

Now $\theta(u,t+\tau)-\theta(u,t)$ is Gaussian with mean zero and variance $2\sigma_\theta^2(1-\rho(\tau))$. Here σ_θ^2 is the variance of $\theta(u,t)$. Using properties of the characteristic function of a Gaussian random variable, it follows that

$$R_{ph}(\tau) = \exp\{-\sigma_\theta^2(1-\rho(\tau))\},$$

where $\rho(\tau)$ is the normalized autocorrelation function of $\theta(u,t)$.

We assume that the specification on the downlink transmitter's rms phase error is $10°$, and that it is due mainly to transmitter generated oscillator noise. Then

$$\sigma_\theta^2 = (\frac{2\pi}{36})^2 = .0305 \text{ rad}^2$$

Notice further that

$$E\{e^{j\theta(u,t)}\} = e^{-\sigma_\theta^2/2} = .98$$

Hence the covariance function of $e^{j\theta(u,t)}$ is given by

$$K_{ph}(\tau) = R_{ph}(\tau) - e^{-\sigma_\theta^2}$$

$$= e^{-\sigma_\theta^2}[e^{\sigma_\theta^2 \rho(\tau)} - 1]$$

For our assumed value of phase variance, this is accurately approximated by

$$K_{ph}(\tau) \doteq e^{-\sigma_\theta^2} \sigma_\theta^2 \rho(\tau).$$

The random variable $\exp\{j\theta(u,t)\}$ has a variance-to-squared mean ratio α given by

$$\alpha = e^{\sigma_\theta^2} K_{ph}(0) \doteq \sigma_\theta^2$$

Assuming that $|A(u,t)|$ has the same ratio α and the same normalized spectral shape as $\exp\{j\theta(u,t)\}$, it follows that

$$R_A(\tau) = R_{|A|}(0) R_{ph}^2(\tau).$$

Note that $R_{ph}(0)$ is unity and hence we define

$$R_A(0) = 2E\{s_k^2(t)\} = 2P$$

where P is the average transmitted power of a spacetenna subarray (P is nominally 65 kw), and

$$R_A(\tau) = 2P[K_{ph}(\tau) + e^{-\sigma_\theta^2})^2$$

$$= 2Pe^{-2\sigma_\theta^2}[\alpha\rho(\tau) + 1]^2$$

The mean $\bar{A}$ and covariance function $K_A(\tau)$ required in section 5 are

$$\overline{A} = \sqrt{2P}\, e^{-\sigma_\theta^2}$$

$$K_A(\tau) \approx 4Pe^{-2\sigma_\theta^2}\alpha\rho(\tau)$$

The only parameter which has yet to be specified in this model is the normalized correlation function of the phase noise $\theta(u,t)$.

Our computations actually use the Fourier transform of $K_A(\tau)$, namely $S_A(f)$. Hence

$$S_A(f) \approx 4Pe^{-2\sigma_\theta^2}\alpha S_0(f)$$

where $S_0(f)$ is the Fourier transform of $\rho(\tau)$. Our model for this normalized density is

$$S_0(f) = \begin{cases} C, & |f| < 1 \text{ KHz} \\ C(f/10^3)^{-6}, & 1 \text{ KHz} < |f| < 10 \text{ KHz} \\ 10^{-6}C(f/10^4)^{-2}, & 10 \text{ KHz} < |f| \end{cases}$$

where the normalizing factor C turns out to be

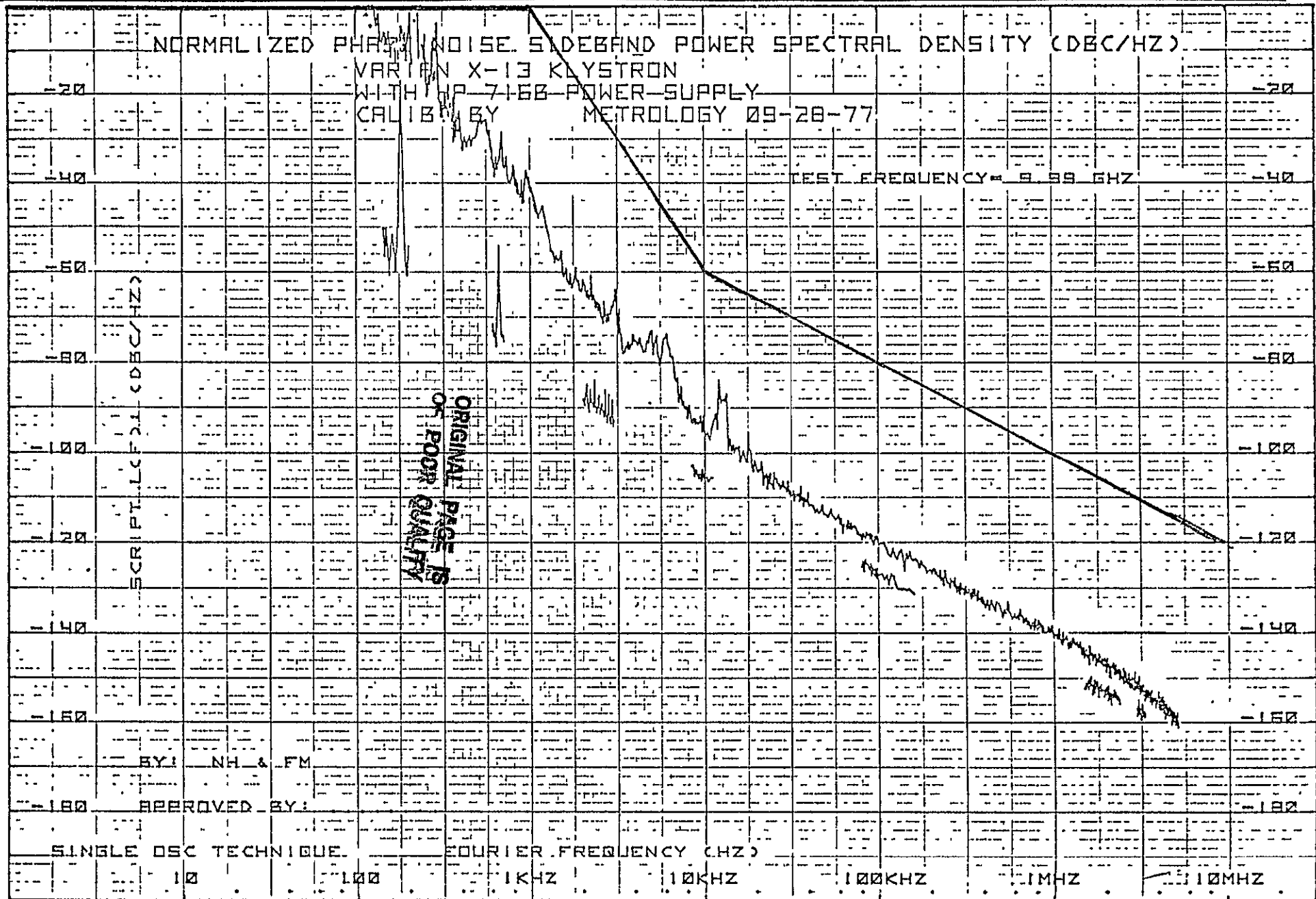$$C = (2.4 \times 10^3)^{-1}.$$

This model is derived from the shape of the spectral density of a Varian X-13 kylstron tube indicated in Fig. A5-1. It is more pessimistic than the klystron data since more power is placed outside 1 KHz. (Presumably, the noise power inside 1 KHz will be notched out and does not affect performance.)

Figure A5-1.   Model for $S_\theta(f)/C$ Based on Varian X-13 Klystron.

APPENDIX 6

OPTIMAL CDMA CODES

This appendix surveys several known sequence sets which may be used as spread spectrum codes in code-division multiple-access communication systems. All of the designs basically achieve Welch's lower bound on the maximum value of periodic cross-correlation between signals and are optimal in this sense.

1. Introduction

In 1974 L. R. Welch [1] published a bound on inner products which could be specialized to the case of periodic correlation of spread-spectrum code-division multiple-access (CDMA) signal sets. Specifically, consider a set of M sequences a_t^i, i = 1,...,M, of period L,

$$a_t^i = a_{t+L}^i \qquad \forall i,t \quad . \tag{A6-1}$$

The periodic cross-correlation between sequence i and sequence j at shift τ is defined as

$$C_{ij}(\tau) \triangleq \sum_{t=0}^{L-1} a_{t+\tau}^i (a_t^j)^* , \tag{A6-2}$$

($(\cdot)^*$ denotes conjugation), the maximum autocorrelation of the set is

$$C_1 \triangleq \max_i \max_{0<\tau<L} |C_{ii}(\tau)| , \tag{A6-3}$$

and the maximum crosscorrelation of the set is

$$C_2 \triangleq \max_{i\neq j} \max_{0\leq\tau<L} |C_{ij}(\tau)| . \tag{A6-4}$$

Under the assumption that the sequences all have the same "energy" per period, i.e.,

$$C_{ii}(0) = C_{jj}(0) \quad \forall i,j \quad , \qquad (A6\text{-}5)$$

Welch demonstrates the normalized correlation bound

$$C_{max} \triangleq \frac{max(C_1,C_2)}{C_{11}(0)} \geq \sqrt{\frac{M-1}{ML-1}} \quad . \qquad (A6\text{-}6)$$

This bound has become the standard against which a possible CDMA

signal set design is compared, despite the fact that C_{max} often

is not specifically a parameter in the communication system design [2].

The purpose of this Appendix is to review several of the CDMA

sequence designs which are known to nearly achieve the Welch bound.

2. Optimal CDMA Code Designs

A. Kasami Sequences [3,4] were designed originally as a linear cyclic

error-correcting codes. The underlying arithmetic in Kasami's design is

performed in the finite field $GF(2^n)$, n even, with $M_1(z)$ representing

the minimum polynomial over $GF(2)$ of a primitive element α of $GF(2^n)$,

and $m_s'(z)$ representing the minimum polynomial over $GF(2)$ of α^s , where

$s = 2^{n/2}+1$. Thus α has order $2^{n/2}-1$ and is a primitive element of

$GF(2^{n/2})$. Hence $M_1(z)$ and $M_s(z)$ can be viewed as the characteristic

polynomials of binary $(0,1)$ linear feedback shift registers which

generate m-sequences, b_t^1 and b_t^3 of lengths 2^n-1 and $2^{n/2}-1$ respectively.

The Kasami sequence set consists of linear combinations of the two

sequences which, after converting to ± 1 sequences, are

$$a_t^i = (-1)^{b_t^1+b_{t+i}^s}, \quad \forall t,i = 1,\dots,2^{n/2}-1 \qquad (A6\text{-}7)$$

and

$$a_t^{2^{n/2}} = (-1)^{b_t^1}$$

This yields a set of

$$M = 2^{n/2} \tag{A6-8}$$

sequences, all with period

$$L = 2^n - 1 \tag{A6-9}$$

and

$$\max(C_1, C_2) = 2^{n/2} + 1 \quad . \tag{A6-10}$$

B.   Bent sequences [5,6] posses an underlying arithmetic structure in $GF(2^n)$, n divisible by 1, which is linked to the space V_n of binary n-tuples over GF(2) by a basis $\beta_1, \beta_2, \dots, \beta_n$ for $GF(2^n)$ which has the property that

$$tr(\beta_i \beta_j) = \begin{cases} 1 \ , & i = j \\ 0 \ , & \text{otherwise} \end{cases} \tag{A6-11}$$

Here $tr(\cdot)$ represents the trace function mapping $GF(2^n)$ onto GF(2) [7]. This generates a correspondence between discrete Fourier transforms of functions defined on V_n and trace transforms of the same functions defined on $GF(2^n)$. This property is exploited along with the fact that bent functions [8] on V_n have a flat Fourier transform to eventually give the following set of sequences:

$$a_i^t = (-1)^{G(\underline{Y}_1) + \underline{Y}_1^T \underline{Y}_2 + \underline{C}^T \underline{X} + \underline{I}^T \underline{Y}} \tag{A6-12}$$

where $\underline{X}$ is the (vector) contents at time t of a Galois-configured linear-feedback shift-register with a primitive characteristic polynomial of degree n,

$$\underline{Y} \triangleq \begin{bmatrix} \underline{Y}_1 \\ \underline{Y}_2 \end{bmatrix} = L\underline{X} \tag{A6-13}$$

where L is a specially designed n/2 x n matrix, the dimension of $\underline{Y}_1$
and $\underline{Y}_2$ being n/4, I is the representation of i as a binary n/2-tuple
$\underline{C}$ is a fixed non-zero constant and $G(\underline{Y}_1)$ is a fixed arbitrary Boolean
Function of $\underline{Y}_1$. This design results in a set of sequences with the
same M,L, and $\max(C_1,C_2)$ parameters as the Kasami sequences (see (8)-
(10)).

C. Group character sequences [9,11] are based on properties of the
group M(L) of integers relatively prime to L under multiplication
modulo L. In the special case when L is a prime, then

$$a_t^i \; = \; \begin{cases} 0 \; , & t = 0 \\ \rho^{i\ell(t)}, & 0 < t < L, \end{cases} \qquad (A6\text{-}14)$$

where ρ is a primitive L-1st root of unity and $\ell(t)$ is the modulo L
logarithm of t in the sense that

$$g^{\ell(t)} \; = \; t \text{ modulo } L \; , \qquad (A6\text{-}15)$$

g being a primitive element of M(L). The index i is restricted to
$1 \le i < L-1$. Of course for large values of L the use of $a_0^1 = 1$ will
make little difference in the final results. Group character sequences
have the following properties:

$$\begin{aligned} M &= L-2 \\ L &= \text{prime number} \\ C_1 &= 1 \\ C_2 &= \sqrt{L} \\ C_{11}(0) &= L-1 \end{aligned} \qquad (A6\text{-}16)$$

Generally, the ith sequence is composed of $(L-1)/\gcd(i,L-1)$ order roots
of unity, e.g., $i = (L-1)/2$ is a sequence of ±1's and is usually called

a quadratic residue sequence.

D. Welch and Alltop separately have proposed (unpublished to my knowledge) signal designs which incorporate a cyclic difference set structure [12] to determine the locations of the non-zero elements of a sequence. A (v,k,λ) cyclic difference set is a collection $\{t_j\}$ of integers in the range $0 \leq d_j < v$ with the property that the equation

$$t_i - t_j = \ell \bmod v \qquad (A6-17)$$

has λ solutions for $\ell \neq 0$ and k solutions when $\ell = 0$. We view the elements of the difference set as the times t at which the sequence elements are non-zero. The values of the non-zero elements of each sequence are chosen so that any pair of sequences is orthogonal or nearly orthogonal when the shift parameter τ is zero.

For example let $\{x_t\}$ be an m-sequence over GF(q), i.e., it satisfies an nth order linear recursion over GF(q) and has period $q^n - 1$. Then a cyclic difference set with parameters

$$v = \frac{q^n - 1}{q - 1} \quad , \quad k = \frac{q^{n-1} - 1}{q - 1} \quad , \quad \lambda = \frac{q^{n-2} - 1}{q - 1} \quad , \qquad (A6-18)$$

is given by

$$\mathscr{D} = \{t : x_t = 0\} \qquad (A6-19)$$

If we consider a set of sequences based on the above difference set with n = 3, then the resulting design parameters are

$$C_{11}(0) = \begin{aligned} L = v &= q^2 + q + 1 \\ M = k &= q + 1 \\ \max(C_1, C_2) = \lambda &= 1. \end{aligned} \qquad (A6-20)$$

Orthogonality of the sequences at $\tau = 0$ imposes the result M=k. When q

$C \doteq 2$

is one less than a multiple of 4, then the rows of a Hadamard

matrix [13] can supply the appropriate modulation. In this case if

the $L_j\underline{th}$ entry in the $(q+1) \times (q+1)$ Hadamard matrix is denoted by b_{ij},

and the elements of the difference set are $t_1,\ldots,t_M$, then

$$a_{t_j}^i = \begin{cases} b_{ij} & 1 \le i \le M, \ 1 \le j \le M \\ 0 & \text{otherwise} \end{cases} \qquad (A6-21)$$

Other similar designs are possible.

E. Discrete Linear FM sequences [14,15] of various types have been

studied. For example,

$$a_t^i = \rho^{it^2}, \quad 0 \le t < L, \ 0 \le i < \rho(L) \qquad (A6-22)$$

where L is an odd number, ρ is a primitive L-$\underline{th}$ root of unity, and $\rho(L)$

is the smallest prime divisor of L. When L is prime,

$$L = \rho(L) \qquad (A6-23)$$

and, using Gaussian sums, it can be shown that

$$C_{max} = L^{-1/2} \qquad (A6-24)$$

In addition to this design Alltop [15] suggests optimal designs based

on phase functions which are proportional to t^3 and based on difference

sets (although sequence elements all have unit magnitude).

3. Comparisons

It appears that there are many designs which asymptotically

achieve the Welch bound on correlation as the sequence period L increases.

How does one choose a CDMA signal set design from among the class of

"optimal" designs?

If you are restricted to binary (± 1) modulation, the obvious

candidates are the Kasami sequences and the bent function sequences.

The choice may be dictated by L which is 4^k-1 for Kasami sequences and 16^k-1 for bent sequences, k being an arbitrary integer in each case. The sequences are comparable in terms of implementation complexity for the same L but the bent sequence set has two distinct disadvantages:

(1) The Kasami sequences have a linear span on the same order of 3n when $GF(2^n)$ is the basic field, while bent sequences apparently have linear spans which can nearly achieve Key's upper bound [16],

$$\sum_{i=1}^{d} \binom{n}{i} \qquad (A6\text{-}25)$$

where d is the degree of the bent function ($d \leq n/4$ depending on the function chosen).

(2) All of the Kasami sequences are generated by the same hardware, with choice of sequence made by initializing register contents. Thus it is difficult to initialize a generator to begin producing a copy of a particular Kasami sequence at some arbitrary point within the sequence. On the other hand bent sequence generators have "time" controlled by a shift register and sequence selection performed by an independent setting. Hence bent sequence generators are easily set to produce a given sequence.

It is worth noting that Gold codes [17] which are now in use in several systems, e.g., [18], have the same drawbacks as Kasami sequences. In addition, while Gold codes are a larger collection ($M=2^n+1$) of binary sequences for the same period ($L=2^n-1$), they do not come close to achieving the Welch bound.

LinCom

The ability to generate and correlate multiphase sequences considerably enlarges the variety of periods L for which optimal designs are known. The number of distinct phases which must be handled is a function of the number of sequences actually required as well as the period length. For example the group character sequences of length L=257 are composed in general of 256th roots of unity, but the ith sequence in the set is made up of 256/gcd(256,i)th roots of unity. Hence in this case the 128th sequence is the binary quadratic residue sequence, the 64th and 192th sequences are composed of 4th roots of unity, and in general there are 2^{k-1} sequences using 2^kth roots of unity k=1,...,7, with the remainder using some primitive 256th roots of unity.

In comparing the group character sequences with the discrete linear FM sequences, one must consider the problem of mechanization for large L. The FM sequences have a relatively simple algorithm (A6-22) for determining the phase of each bit. On the other hand group character sequence generation is based on computing the logarithm of t modulo L-1. In most cases this is a difficult computation [19].

The main detractions of the difference set design are: (1) irregularity of the transmitter power, and (2) the requirement of phase coherence, despite the on-off nature of the signal. The orthogonal ±1 modulation of the non-zero pulses is easily achieved, especially when the number k of pulses per period is a power of 2.

Ultimately, with the variety of designs available, it appears that convenience of mechanization may very well be the deciding factor in a design.

LinCom

REFERENCES

[1] L. R. Welch, "Lower Bounds on the Maximum Cross Correlation of Signals," IEEE Trans. on Inform. Theory, Vol. IT-20, No. 3, May 1974, pp. 397-399.

[2] M. B. Pursley and D. V. Darwate, "Performance Evaluation for Phase-Coded Spread-Spectrum Multiple-Access Communication--Part II: Code Sequence Analysis," IEEE Trans. on Communications, Vol. COM-25, No. 8, August 1977, -p. 800-803.

[3] T. Kasami, "Weight Distribution Formula for Some Class of Cyclic Codes," Coordinated Science Laboratory, Univ. of Illinois Report R-285, April 1966.

[4] H. F. A. Roefs, "Binary Sequences for Spread-Spectrum Multiple-Access Communication," Coordinated Science Laboratory, Univ of Illinois, Report R-785, April 1977.

[5] J. D. Olsen, "Non-linear Binary Sequences with Asymptotically Optimum Periodic Cross-Correlation," Dissertation, University of Southern California, Dec. 1977.

[6] J. D. Olsen, R. A. Scholtz and L. R. Welch, "Bent Function Sequences," submitted to IEEE Trans. Inform. Theory.

[7] E. R. Berlekamp, Algebraic Code Theory, New York: McGraw-Hill, 1968.

[8] O. S. Rothaus, "On Bent Functions," Journal of Combinational Theory, Series A20, pp. 300-350, 1976.

[9] R. M. Lerner, "Signals Having Good Correlation Functions," IEEE WESCON Convention Record, 1961.

[10] R. A. Scholtz and L. R. Welch, "Generalized Residue Sequence," ICC Conference Record, June 1973.

[11] R. A. Scholtz and L. R. Welch, "Group Characters, Sequences with Good Correlation Properties," IEEE Trans. on Inform. Theory, Vol. IT-24, No. 5, Sept. 1978, pp. 537-545.

[12] L. D. Baumert, Lecture Notes in Mathematics--Cyclic Difference Sets, Springer-Verlag, 1971.

[13] W. D. Wallis, A. D. Street, and J. S. Wallis, Lecture Notes in Mathematics-Combinatorics: Room Squares, Sum-Free Sets, Hadamard Matrices, Springer-Verlag, 1972.

[14] D. C. Chu, "Polyphase Codes with Good Periodic Correlation Properties," IEEE Trans. Inform. Theory, Vol. IT-18, July 1972, pp. 531-532.

[15] W. O. Alltop, "Complex Sequences with Low Periodic Correlations," to be published in the IEEE Trans. on Inform. Theory.

[16] E. L. Key, "An Analysis on the Structure and Complexity of Non-linear Binary Sequence Generators," IEEE Trans. on Inform. Theory, Vol. IT-22, Nov. 1976, pp. 732-736.

[17] R. Gold, "Optimal Binary Sequences for Spread Spectrum Multiplexing," IEEE Trans. on Inform. Theory, Vol. IT-13, No. 4, Oct. 1967, pp. 619-621.

[18] J. J. Spilker, Jr., "GPS Signal Structure and Performance Char-acteristics," Navigation, Vol. 25, No. 2, Summer 1978, pp. 121-146.

[19] S. C. Pohlig and M. E. Hellman, "An Improved Algorithm for Computing Logarithms over GF(p) and Its Cryptographic Significance," IEEE Trans. on Inform. Theory, Vol. IT-24, No. 1, Jan. 1978, pp. 106-110.

APPENDIX 7

SOLARSIM SUBROUTINE SIDR

The SOALRSIM subroutine SIDR is developed to compute the Costas loop phase jitter as a function of the pilot signal and RF front end parameters. Figure A7-1 is a sample run for SIDR. The inputs to the program are described as follows:

F3 – 3 dB bandwidth of the RF filter normalized to the chip rate R_c

DELTA – 3 dB bandwidth of the notch filter normalized to R_c

GAMMA – γ^2 is the notch filter attenuation at band center

M – PN code length

K1 – Coupling coefficient for noncoherent phase noise

K2 – Coupling coefficient for coherent phase noise

The other inputs are self explanatory from Fig. A7-1. There are some intermediate outputs besides the resultant Costas loop phase jitter SIGMA. They are:

POWER – Received pilot signal power in W

ALPHA – Time constant of the RF filter normalized to R_c

TC – Chip time

NEQ – Equivalent thermal noise level after despread

L_F – Fractional loss in pilot signal power

A software package is also developed to plot the computer output (as shown in Figs. 11.1-11.5) on an HP-plotter.

```
ENTER NUMBER OF ELEMENTS OF F3,DELTA,GAMMA,M,RC :
(ONE FLOATING POINT ENTRY FOR LINE)
1.
1.
1.
1.
1.
ENTER VALUES FOR RF FILTER 3DB BANDWIDTH IN FRACTION OF RC (F3) :
2.
ENTER VALUES FOR DELTA :
.1
ENTER VALUES FOR GAMMA :
.001
ENTER VALUES FOR M :
10000.
ENTER VALUES FOR CHIP RATE IN MHZ (RC) :
10.
ENTER  K1 :
.01
ENTER  K2 :
.01
(FOR THE FOLLOWING, HIT RETURN FOR NOMINAL VALUES, OTHERWISE ENTER DESIRED VALUE)

ENTER CHIP BIAS E IN % (NOMINAL 10)

ENTER LOOP BANDWIDTH IN HZ (NOMINAL 10) :

ENTER  TRANSMIT POWER IN KW (NOMINAL  65) :

ENTER PER CENT OF TRANSMIT EFFICIENCY (NOMINAL  50) :

ENTER VALUE FOR DIAMETER OF TRANSMIT ANTENNA AREA IN METER (NOMINAL  10) :

E=  0.1000      BL=  10.0000
POWER= 0.354033E-06
K1=  0.010000    K2=  0.010000
GAMMA =   0.001000


ALPHA=  0.079577
DELTA= 0.9999996E-01
M=  10000.0
RC =  10.0000        TC= 0.100000E-06
NEQ= 0.441106E-13
LF= 0.643650        SIGMA- 0.104654
```

Figure A7-1. A Sample Run of the Program SIDR in SOLARSIM.